A high angular resolution survey of massive stars in Cygnus OB2 : JHK adaptive optics results from the Gemini Near-Infrared Imager.

Article:

Caballero-Nieves, S.M., Gies, D.R., Baines, E.K. et al. (8 more authors) (2020) A high angular resolution survey of massive stars in Cygnus OB2 : JHK adaptive optics results from the Gemini Near-Infrared Imager. The Astronomical Journal, 160 (3). 115. ISSN 0004-6256

https://doi.org/10.3847/1538-3881/aba536

Draft version August 4, 2020
Typeset using LaTeX **preprint** style in AASTeX63

A High Angular Resolution Survey of Massive Stars in Cygnus OB2: JHK Adaptive Optics Results from the Gemini Near-InfraRed Imager

S. M. Caballero-Nieves,[1] D. R. Gies,[2] E. K. Baines,[3] A. H. Bouchez,[4,5] R. G. Dekany,[6] S. P. Goodwin,[7] E. L. Rickman,[8] L. C. Roberts Jr.,[9] K. Taggart,[10] T. A. ten Brummelaar,[11] and N. H. Turner[11]

[1] *Department of Physics and Space Sciences, Florida Institute of Technology 150 University Blvd, Melbourne, FL 32901, USA*

[2] *Center for High Angular Resolution Astronomy, Department of Physics and Astronomy, Georgia State University, P. O. Box 5060, Atlanta, GA 30302-5060, USA*

[3] *Remote Sensing Division, Naval Research Laboratory, 4555 Overlook Avenue SW, Washington, DC 20375, USA*

[4] *GMTO Corporation, 251 South Lake Avenue, Pasadena, CA 91101,USA*

[5] *Observatories of the Carnegie Institution for Science, 813 Santa Barbara Street, Pasadena, CA 91101, USA*

[6] *California Institute of Technology, 1200 East California Boulevard, Pasadena, CA 91125, USA*

[7] *Department of Physics and Astronomy, University of Sheffield, Hicks Building, Hounsfield Road, Sheffield, S3 7RH, United Kingdom*

[8] *Geneva Observatory, University of Geneva, Chemin des Maillettes 51, CH-1290 Sauverny, Switzerland*

[9] *Jet Propulsion Laboratory, California Institute of Technology, 4800 Oak Grove Drive, Pasadena, CA 91109, USA*

[10] *Astrophysics Research Institute, Liverpool John Moores University, IC2, Liverpool Science Park, 146 Brownlow Hill, Liverpool, L3 5RF, UK*

[11] *The CHARA Array, Mount Wilson Observatory, Mount Wilson, CA 91023, USA*

ABSTRACT

We present results of a high angular resolution survey of massive OB stars in the Cygnus OB2 association that we conducted with the NIRI camera and ALTAIR adaptive optics system of the Gemini North telescope. We observed 74 O- and early B-type stars in Cyg OB2 in the JHK infrared bands in order to detect binary and multiple companions. The observations are sensitive to equal-brightness pairs at separations as small as $0\farcs08$, and progressively fainter companions are detectable out to $\triangle K = 9$ mag at a separation of $2''$. This faint contrast limit due to readnoise continues out to 10 arcsec near the edge of the detector. We assigned a simple probability of chance alignment to each companion based upon its separation and magnitude difference from the central target star and upon areal star counts for the general star field of Cyg OB2. Companion stars with a field membership probability of less than 1% are assumed to be physical companions. This assessment indicates that 47% of the targets have at least one resolved companion that is probably gravitationally bound. Including known spectroscopic binaries, our sample includes 27 binary, 12 triple, and 9 systems with four or more components. These results confirm studies of high mass stars in other environments that find that massive stars are born with a high multiplicity fraction. The results are important for the placement of the stars in the H-R diagram, the interpretation of their spectroscopic analyses, and for future mass determinations through measurement of orbital motion.

Keywords: techniques: high angular resolution — binaries: visual — stars: early-type — stars: massive — open clusters and associations: individual: Cyg OB2

1. INTRODUCTION

Massive stars profoundly influence the evolution of the Universe, from galactic dynamics and structure to star formation. They are often found with bound companions. Massive stars have a higher frequency of multiplicity than cooler, less massive stars (Raghavan et al. 2010; Duchêne & Kraus 2013), especially when they are found in clusters (Mason et al. 2009). Spectroscopic studies of massive stars in the Milky Way (Sana et al. 2012) and in the Tarantula Nebula region of the Large Magellanic Cloud (Sana et al. 2013) demonstrate that perhaps 75% of massive O-type stars have binary companions in orbits small enough that the stars will interact over their lifetime. Our knowledge of O-type multiple systems in larger orbits with periods in the range from years to thousands of years is incomplete due their great distances, but high angular resolution methods are beginning to fill in this period gap (Maíz Apellániz et al. 2019; Le Bouquin et al. 2017; Aldoretta et al. 2015; Sana et al. 2014).

At a distance of 1.33 – 1.7 kpc (Massey & Thompson 1991; Torres-Dodgen et al. 1991; Hanson 2003; Rygl et al. 2012; Kiminki et al. 2015), Cygnus OB2 = Cyg OB2 is the second closest OB association (after Ori OB1) that provides us with an example of a nearby, young stellar environment, rich in high-mass stars. Due to uneven extinction towards the region (Wright et al. 2015), the cluster begins to be unveiled in the infrared (IR). Torres-Dodgen et al. (1991) estimate the age of the association to be least 3 Myr through analysis of their Strömgren and infrared photometry, and Wright et al. (2015) argue that star formation has occurred more or less continuously over the last 1 to 7 Myr based upon the positions of the stars in the Hertzsprung - Russell (H-R) diagram. The young nature of the association is further established by the detection of X-rays from young, low mass stars in the region (Albacete Colombo et al. 2007; Wright & Drake 2009; Wright et al. 2012). Spectroscopic surveys by Massey & Thompson (1991), Hanson (2003), and Kiminki et al. (2007) have established the early-type classifications of these stars. Massive stars are short-lived and therefore spend most of their formative years shrouded in their natal clouds, so that when they shed these clouds and a hot star is revealed, it is usually well into the main sequence stage of its life. The multiplicity of massive stars must play an important role in their formation because so many are members of binary systems (Zinnecker & Yorke 2007). Massive stars are formed through the turbulent core collapse of a single cloud or by competitive accretion of multiple stellar seeds in a dense cloud (see the review by Rosen et al. 2020), and models of these processes predict a large incidence of binary stars with specific distributions of mass ratio and separation (Peter et al. 2012; Gravity Collaboration et al. 2018). Therefore, by studying the multiplicity properties of massive stars at an early stage we can test the role of companions in formation theories of massive stars.

The Cyg OB2 association is close enough that with modern-day adaptive optics (AO) we are able to resolve relatively close companions. The ALTAIR AO system and the Near-InfraRed Imager and Spectrograph (NIRI) at the Gemini North Observatory provides an effective tool to search for binaries, as was demonstrated by Lafrenière et al. (2014) in a multiplicity study of young stars in the Upper Sco association. With a resolution of $\sim 0\farcs06$ and a sensitivity contrast limit of about

10 mag for differential photometry, the ALTAIR AO infrared system can delve into the depths of the association and find faint companions with periods in the range from hundreds to thousands of years. Our results complement the radial velocity survey of Kobulnicky et al. (2014) (and references therein) who searched for short period, spectroscopic systems in Cyg OB2. They determined that 30% of their sample are spectroscopic binaries with periods less than 45 days.

In this paper, we provide measurements of JHK-band relative photometry and positions of candidate companions to our target stars. These results provide the first step in determining the true multiplicity fraction of widely separated systems. In section 2 we describe the observations of the sample in Cygnus OB2. We present the results of the survey in section 3 along with further details of the calibration in appendices for the astrometry (Appendix A) and photometry (Appendix B). We discuss the detection limits and the identification of probable physical companions in section 4. Section 5 presents the multiplicity fraction and companion frequency for the Cyg OB2 sample and compares these to similar results from studies of massive stars in other locations. We summarize the results and their significance in section 6.

2. OBSERVATIONS

We were able to observe 74 of the brightest O- and B-type stars in Cyg OB2 and one misidentified non-member using the infrared ALTAIR AO system (Richardson et al. 1998; Roberts & Singh 1998a) at the Gemini North Observatory. We provide a list of our targets in Table 1 (given in full in the electronic version) that gives the target name, celestial coordinates (J2000), spectral classification and reference, optical and infrared (IR) magnitudes, and three measures of interstellar reddening. The majority of stars in this study were selected from the optical survey of Massey & Thompson (1991), who presented Johnson B and V magnitudes for the brighter stars in the sample as well as reddening towards each star. These targets are identified with prefix "MT" by their number assigned by Massey & Thompson (1991). Seventeen of our targets were selected from the infrared surveys by Comerón et al. (2002, 2008), and these are referenced by a prefix "A" or "B" from those papers. These are redder sources that are not readily detected in the optical surveys, but V-band and spectral information are available for some of these from Straižys & Laugalys (2008). An "S" designation is given for three stars from the compilation by Schulte (1958), and the final object is given by its Wolf-Rayet catalog number (van der Hucht 2001). The spectral classifications are taken from a variety of sources, indicated in the notes below the table. The V magnitudes reported are from Massey & Thompson (1991) for the MT # stars and from Straižys & Laugalys (2008) for others. The coordinates and infrared JHK_s photometry are from the Two Micron All Sky Survey (2MASS; Skrutskie et al. 2006). The reddening estimates are discussed in section 4.3 below. After we completed our observations we learned that the object MT 140 is in fact an intermediate mass object that is not a member of Cyg OB2 (Maíz Apellániz et al. 2016). We include our measurements here for completeness, but it is excluded from the multiplicity analysis.

Wright et al. (2015) describe the massive star content of the Cyg OB2 association, and they suggest that the association hosts 52 O-type stars and 3 Wolf-Rayet stars. Our sample includes 56 O-type stars and one Wolf-Rayet star, plus a number of luminous and/or early type B-stars. Thus, our target list should represent an almost complete sample of the most massive stars ($M/M_\odot > 18$) in Cyg OB2 (missing the Wolf-Rayet Stars WR 144 and WR 146).

Table 1. Sample of Stars in Cygnus OB2

Star Name	Schulte #	R.A. (HH:MM:SS)	Dec. (DD:MM:SS)	Spectral Classification	Class. Ref.	V (mag)	J (mag)	H (mag)	K_s (mag)	$E(J-K)$ (mag)	$E(B-V)$ (mag)	$E(b-y)$ (mag)
A 11	(MT 267)	20:32:31.539	+41:14:08.22	O7.5 III-1	1	···	7.817	7.094	6.664	1.32	···	···
A 12		20:33:38.219	+40:41:06.41	B0 Ia	3	···	6.904	6.170	5.745	1.40	···	···
A 15		20:31:36.909	+40:59:09.25	O7 Ib(f)	3	···	7.913	7.208	6.811	1.32	···	···
A 18		20:30:07.879	+41:23:50.47	O8 V	3	···	9.397	8.739	8.365	1.25	···	···
A 20		20:33:02.920	+40:47:25.45	O8 II((f))	5	···	7.251	6.632	6.274	1.16	···	···
A 23		20:30:39.710	+41:08:48.98	B0.7	5	···	6.928	6.328	5.980	1.08	···	···
A 24		20:34:44.110	+40:51:58.51	O6.5 III((f))	3	···	8.405	7.796	7.448	1.15	···	···
A 25		20:32:38.441	+40:40:44.54	O8 III	3	···	8.347	7.705	7.383	1.19	···	···
A 26		20:30:57.730	+41:09:57.57	O9.5 V	3	···	9.093	8.514	8.198	1.14	···	···
A 27		20:34:44.719	+40:51:46.56	B0 Ia	3	···	6.683	6.062	5.731	1.14	···	···
A 29		20:34:56.061	+40:38:18.06	O9.7 Iab	5	···	7.440	6.859	6.545	1.05	···	···
A 32		20:32:30.330	+40:34:33.26	O9.5 IV	5	···	7.892	7.365	7.070	1.01	···	···
A 37		20:36:04.520	+40:56:12.98	O5 V	5	···	8.568	7.968	7.685	1.04	···	···
A 38		20:32:34.870	+40:56:17.42	O8 V	3	···	9.382	8.858	8.564	0.98	···	···
A 41		20:31:08.378	+42:02:42.28	O9.7 II	5	···	7.828	7.292	7.023	0.96	···	···
A 46		20:31:00.200	+40:49:49.75	O7 V	5	···	8.378	8.016	7.826	0.70	···	···
B 17		20:30:27.299	+41:13:25.31	O7:	1	···	7.630	6.850	6.445	···	···	···
MT 5		20:30:39.820	+41:36:50.72	O6 V	2	12.93	9.098	8.574	8.313	0.95	1.96	···
MT 59	CygOB2-1	20:31:10.549	+41:31:53.55	O8 V	1	11.06	7.968	7.556	7.365	0.76	1.78	1.20
MT 70		20:31:18.330	+41:21:21.66	O9 II	1	12.99	8.607	8.046	7.746	1.04	2.41	···
MT 83	CygOB2-2	20:31:22.038	+41:31:28.41	B1 I	2	10.61	8.075	7.750	7.628	0.58	1.37	1.01
MT 138		20:31:45.400	+41:18:26.75	O8 I	2	12.26	8.065	7.552	7.259	0.99	2.27	1.49
MT 140*		20:31:46.011	+41:17:27.07	F	5	9.38	8.240	8.061	8.048	···	···	···
MT 145	CygOB2-20	20:31:49.659	+41:28:26.52	O9 III	1	11.62	9.074	8.768	8.634	0.62	1.41	0.99
MT 213		20:32:13.130	+41:27:24.63	B0 V	2	11.95	9.521	9.248	9.071	0.63	1.43	···
MT 217	CygOB2-4	20:32:13.830	+41:27:12.03	O7 IIIf	2	10.07	7.582	7.248	7.105	0.67	1.50	1.03
MT 227	CygOB2-14	20:32:16.560	+41:25:35.71	O9 V	2	11.47	8.714	8.389	8.185	0.71	1.55	1.06
MT 250		20:32:26.079	+41:29:39.36	B2 III	2	12.88	10.427	10.150	9.993	0.61	1.32	···
MT 258	CygOB2-15	20:32:27.660	+41:26:22.08	O8 V	1	10.90	8.535	8.193	8.021	0.67	1.51	1.04
MT 259	CygOB2-21	20:32:27.739	+41:28:52.28	B0 Ib	2	11.50	9.191	8.895	8.766	0.57	1.28	0.90
MT 299	CygOB2-16	20:32:38.579	+41:25:13.75	O7 V	2	11.12	8.194	7.918	7.716	0.63	1.50	1.03

Table 1 *continued on next page*

Table 1 *(continued)*

Star Name	Schulte #	R.A. (HH:MM:SS)	Dec. (DD:MM:SS)	Spectral Classification	Class. Ref.	V (mag)	J (mag)	H (mag)	K_s (mag)	$E(J-K)$ (mag)	$E(B-V)$ (mag)	$E(b-y)$ (mag)
MT 304	CygOB2-12	20:32:40.958	+41:14:29.16	B3 Iae	2	11.40	4.667	3.512	2.704	···	3.44	···
MT 317	CygOB2-6	20:32:45.458	+41:25:37.43	O8 V	2	10.65	7.953	7.617	7.421	0.69	1.56	1.07
MT 339	CygOB2-17	20:32:50.019	+41:23:44.68	O8 V	2	11.71	8.579	8.188	7.982	0.76	1.66	1.15
MT 376		20:32:59.190	+41:24:25.50	O8 V	2	11.91	8.886	8.524	8.314	0.73	1.66	1.13
MT 390		20:33:02.920	+41:17:43.14	O8 V	2	12.95	8.718	8.165	7.873	1.01	2.29	1.51
MT 403		20:33:05.269	+41:43:36.80	B1 V	2	12.94	9.286	8.854	8.624	0.81	1.74	···
MT 417	CygOB2-22	20:33:08.801	+41:13:18.21	O3 I	6	11.68	7.110	6.540	6.226	1.08	2.36	1.60
MT 421	CygOB2-50	20:33:09.600	+41:13:00.54	O9 V	1	12.86	8.655	8.135	7.764	···	2.26	1.50
MT 429		20:33:10.508	+41:22:22.44	B0 V	1	12.98	9.537	9.113	8.897	0.82	1.86	···
MT 431	CygOB2-9	20:33:10.751	+41:15:08.20	O5:	1	10.78	6.468	5.897	5.570	1.09	2.11	1.52
MT 448		20:33:13.258	+41:13:28.74	O6 V	2	13.61	8.982	8.346	8.009	1.13	2.47	···
MT 455		20:33:13.690	+41:13:05.79	O8 V	2	12.92	9.034	8.559	8.280	0.91	2.12	···
MT 457	CygOB2-7	20:33:14.110	+41:20:21.81	O3 If	2	10.50	7.248	6.818	6.611	0.83	1.76	1.23
MT 462	CygOB2-8B	20:33:14.759	+41:18:41.63	O7 III-II	2	10.70	7.209	6.762	6.570	0.83	1.75	1.13
MT 465	CygOB2-8A	20:33:15.079	+41:18:50.45	O5.5 I	1	8.99	6.123	5.721	5.503	0.81	1.60	1.09
MT 470	CygOB2-23	20:33:15.708	+41:20:17.20	O9 V	2	12.61	9.333	8.935	8.725	0.79	1.76	1.22
MT 473	CygOB2-8D	20:33:16.338	+41:19:01.80	O8.5 V	2	12.02	8.842	8.424	8.239	0.78	1.76	1.14
MT 480	CygOB2-24	20:33:17.479	+41:17:09.31	O7 V	2	11.86	8.354	7.889	7.649	0.85	1.90	1.31
MT 483	CygOB2-8C	20:33:17.989	+41:18:31.10	O5 III	2	10.08	7.165	6.792	6.579	0.79	1.54	1.11
MT 485		20:33:18.030	+41:21:36.65	O8 V	2	11.82	8.744	8.315	8.113	0.79	1.82	1.25
MT 507		20:33:21.020	+41:17:40.14	O9 V	2	12.70	9.301	8.899	8.672	0.81	1.85	1.39
MT 516		20:33:23.458	+41:09:13.00	O5.5 V	2	11.84	7.025	6.380	6.050	1.14	2.52	1.75
MT 531	CygOB2-25	20:33:25.558	+41:33:27.00	O8.5 V	2	11.58	8.168	7.748	7.523	0.83	1.88	1.27
MT 534		20:33:26.748	+41:10:59.51	O8.5 V	2	13.00	8.971	8.434	8.165	0.99	2.18	···
MT 555	CygOB2-74	20:33:30.310	+41:35:57.89	O8 V	2	12.51	8.385	7.839	7.568	0.98	2.21	···
MT 556	CygOB2-18	20:33:30.790	+41:15:22.66	B1 I	2	11.01	6.493	5.891	5.542	1.08	1.96	1.55
MT 588	CygOB2-70	20:33:37.000	+41:16:11.30	B0 V	2	12.40	8.683	8.168	7.929	0.93	1.96	1.40
MT 601	CygOB2-19	20:33:39.110	+41:19:25.86	B0 Iab	2	11.06	7.230	6.745	6.482	0.89	1.77	1.32
MT 605		20:33:39.798	+41:22:52.37	B1 V	1	11.78	8.876	8.543	8.279	0.75	1.47	1.08
MT 611		20:33:40.869	+41:30:18.98	O7 V	2	12.77	9.263	8.866	8.614	0.80	1.88	1.27
MT 632	CygOB2-10	20:33:46.100	+41:33:01.05	O9 I	2	9.82	6.294	5.839	5.582	0.87	1.86	1.28
MT 642	CygOB2-26	20:33:47.839	+41:20:41.54	B1 III	2	11.87	7.986	7.487	7.209	0.97	1.79	1.32
MT 692		20:33:59.250	+41:05:38.09	B0 V	2	13.61	9.988	9.567	9.301	0.87	1.99	···
MT 696	CygOB2-27	20:33:59.529	+41:17:35.48	O9.5 V	1	12.25	8.534	8.140	7.889	0.82	1.95	1.32

Table 1 *continued on next page*

Table 1 *(continued)*

Star Name	Schulte #	R.A. (HH:MM:SS)	Dec. (DD:MM:SS)	Spectral Classification	Class. Ref.	V (mag)	J (mag)	H (mag)	K_s (mag)	$E(J-K)$ (mag)	$E(B-V)$ (mag)	$E(b-y)$ (mag)
MT 716		20:34:04.861	+41:05:12.92	O9 V	2	13.50	9.561	9.095	8.836	0.91	2.14	···
MT 734	CygOB2-11	20:34:08.502	+41:36:59.26	O5 I	1	10.08	6.650	6.226	5.990	0.85	1.79	1.19
MT 736	CygOB2-75	20:34:09.520	+41:34:13.70	O9 V	2	12.79	9.304	8.892	8.646	0.84	1.77	···
MT 745	CygOB2-29	20:34:13.509	+41:35:02.74	O7 V	2	12.04	8.550	8.148	7.921	0.78	1.82	1.26
MT 771		20:34:29.600	+41:31:45.55	O7 V	1	11.64	7.560	7.030	6.709	1.00	2.37	···
MT 793	CygOB2-30	20:34:43.580	+41:29:04.63	B2 IIIe	2	12.36	8.614	8.116	7.701	1.09	1.79	1.28
Schulte 3	CygOB2-3	20:31:37.501	+41:13:21.04	O6 IV:	1	10.35	6.498	6.001	5.748	···	···	1.36
Schulte 5	CygOB2-5	20:32:22.431	+41:18:19.10	O7 Ianfp	1	9.21	5.187	4.745	4.339	···	···	1.34
Schulte 73	CygOB2-73	20:34:21.929	+41:17:01.60	O8 III	1	12.50	8.388	7.878	7.602	···	···	1.45
WR 145		20:32:06.289	+40:48:29.54	WN7o/CE	4	12.30	7.373	6.714	6.239	···	2.03	···

References— 1. Kobulnicky et al. (2012); 2. Kiminki et al. (2007); 3. Negueruela et al. (2008); 4. Muntean et al. (2009); 5. http://simbad.u-strasbg.fr/simbad/; 6. Mason et al. (2001).

[*] MT 140 appears to be an erroneous F-type star (Maíz Apellániz et al. 2016). We include the observations in the tables but this object is not included in the final analysis of MF and CF.

Table 2. Filter Information

Instrument	Filter Name	Central Wavelength (μm)	Bandpass (μm)
NIRI	Jcon(112)	1.122	0.009
NIRI	Jcon(121)	1.207	0.018
NIRI	Hcon(157)	1.570	0.024
NIRI	Kcon(209)	2.0975	0.027
PHARO	J	1.246	0.162
PHARO	H	1.635	0.296
PHARO	K_S	2.145	0.310

Our observations were made in three queue observing programs at the 8.1-m Gemini North Observatory during the 2005B, 2008A and 2008B observing semesters. Using the Near InfraRed Imager and Spectrograph (NIRI) with the ALTAIR adaptive optics (AO) system (Hodapp et al. 2003; Richardson et al. 1998; Roberts & Singh 1998b), we collected high resolution images ($0\farcs022$ pixel^{-1} with the $f/32$ camera) with a field of view (FOV) of approximately $22'' \times 22''$. The only exception is for our K-band observations of MT 304 = Cyg OB2 #12. Due to its extreme IR brightness ($K = 2.7$) MT 304 was observed with the shortest exposure time possible, and therefore, a smaller FOV ($11'' \times 11''$) was used so that the data could be read out without over-exposing the images. The detector chip used the deep well setting for improved dynamic range, and the 2008 data were obtained with the ALTAIR field lens which improves the AO correction. The telescope sits on an altitude-azimuth mount, so that when NIRI is held fixed, the sky appears to rotate between frames. For these observations, NIRI was held fixed and the exposure times for each frame ranged between 0.02 s to 800 s in K and between 0.1 s to 1869 s in J, depending of the brightness of the target star in each band in order to reach about half of the full well depth of the detector and achieve uniform S/N ratio measurements of the target stars.

Table 2 provides the central wavelength and the pass band for each filter. Every target was observed with the K continuum filter, Kcon(209), to detect possible companions. The numbering corresponds to the central wavelength in hundreds of angstroms. We followed up on 43 stars with J-band observations to get additional color information on those systems with obvious companions. The 2005 data were obtained using the J continuum filter, Jcon(112). The wider Jcon(121) filter was used for the 2008 observations because the companions appear fainter in the J-band than in the K-band. The seven targets observed during the 2005B semester were also imaged with the H continuum filter, Hcon(157), with the exception of MT 304 which was only observed in J at the time. These filters all have narrow pass bands that were needed because the stars are so bright in the infrared.

Each observation consisted of approximately 90 frames. Table 3 (given in full in the electronic version) lists the observation dates of the beginning of the first exposure and the number of frames combined to produce the final co-added image for each filter. Each target was observed at nine dither positions, set up on a 3×3 grid, offset by about 50 pixels and with 10 exposures at each position. For the cases where the observations were taken over two nights, observations from each night were combined individually and also combined together. For the detection of sources, the images from each night were analyzed separately due to differences in image quality, but only data from one night were used for photometric and astrometric measurements (denoted by *). For A 25 in K and A 41 in J, we analyzed the combined image from both nights (denoted by ^{C}) because they were of comparable quality. The fourth and fifth columns give the Strehl ratio and full-width at half-maximum (FWHM), respectively, of the point spread function associated with the primary target. These were determined using the IDL Strehl ratio meter code[1] written by M. van Dam.

In addition to the NIRI K-band observation, MT 421 was observed with the Palomar High Angular Resolution Optics (PHARO; Hayward et al. 2001) camera and the Palm-3000 AO system (Dekany et al. 2013) on the 5-m Hale telescope in 2009 July. We were able to get observations in all three IR bands, J, H, and K_S, with a field of view comparable to that of NIRI ($\sim 25'' \times 25''$). The filter information for PHARO is also listed in Table 2. The PHARO images provide a pixel scale of $0\farcs025$ pixel^{-1} (Hayward et al. 2001).

Table 3. Observations of Stars in Cyg OB2

Star Name	Date (JD – 2,450,000)	Filter Name	Strehl Ratio	FWHM (mas)	Number of Images
A 11	4741.250	Kcon(209)	0.32	83	91
A 12	4741.242	Kcon(209)	0.32	81	90
A 15	4741.234	Kcon(209)	0.33	80	90
A 18	4741.220	Kcon(209)	0.28	85	90
A 20	4741.210	Kcon(209)	0.16	114	90
A 23	4590.621	Kcon(209)	0.36	76	90
A 24	4741.201	Kcon(209)	0.33	80	90
A 25	4740.329^C	Kcon(209)	0.15	124	69
	4741.197^C	Kcon(209)	0.15	124	22
A 26	4740.292	Kcon(209)	0.19	102	90
A 27	4741.261	Jcon(121)	0.05	105	89
	4593.612	Kcon(209)	0.33	77	90
A 29	4740.283	Kcon(209)	0.31	83	90
A 32	4819.203	Jcon(121)	0.01	159	90
	4740.273	Kcon(209)	0.34	81	90
A 37	4740.264	Kcon(209)	0.37	78	90
A 38	4740.249	Kcon(209)	0.22	105	106
A 41	4742.207^C	Jcon(121)	0.08	82	60
	4746.302^C	Jcon(121)	0.08	82	30
	4593.604	Kcon(209)	0.34	75	90
A 46	4593.594	Kcon(209)	0.25	90	90
B 17	4819.184	Jcon(121)	0.02	142	90
	4740.241	Kcon(209)	0.34	81	90
MT 5	4746.310*	Jcon(121)	0.03	115	90
	4747.218	Jcon(121)	0.03	115	90
	4603.605	Kcon(209)	0.33	81	90
MT 59	4743.249	Jcon(121)	0.04	110	90
	4746.343*	Jcon(121)	0.04	110	90
	4607.571	Kcon(209)	0.21	102	90
MT 70	4817.180	Jcon(121)	0.04	114	90

Table 3 *continued on next page*

---

[1] http://www2.keck.hawaii.edu/optics/aochar/Strehl_meter2.htm

Table 3 *(continued)*

Star Name	Date (JD – 2,450,000)	Filter Name	Strehl Ratio	FWHM (mas)	Number of Images
	4607.580	Kcon(209)	0.21	104	90
MT 83	4804.184	Jcon(121)	0.04	105	90
	4598.615	Kcon(209)	0.20	103	90
MT 138	4747.277	Jcon(121)	0.06	102	90
	4607.590	Kcon(209)	0.20	107	90
MT 140	4740.229	Kcon(209)	0.22	107	63
MT 145	4747.326	Jcon(121)	0.06	101	130
	4620.599	Kcon(209)	0.33	83	90
MT 213	4747.347	Jcon(121)	0.06	98	90
	4605.601	Kcon(209)	0.23	101	90
MT 217	4818.176	Jcon(121)	0.02	138	90
	4607.598	Kcon(209)	0.17	114	90
MT 227	4607.607	Kcon(209)	0.19	109	90
MT 250	4818.189	Jcon(121)	0.04	90	90
	4620.611	Kcon(209)	0.35	83	90
MT 258	4805.184	Jcon(121)	0.03	127	90
	4607.617	Kcon(209)	0.19	109	90
MT 259	4622.597	Kcon(209)	0.34	75	70
MT 299	4748.240*	Jcon(121)	0.08	76	90
	4797.187	Jcon(121)	0.08	76	90
	4603.627	Kcon(209)	0.35	83	90
MT 304	3623.314	Jcon(112)	0.08	84	90
	4801.189	Kcon(209)	0.26	75	90
MT 317	4607.626	Kcon(209)	0.28	85	90
MT 339	4610.621	Kcon(209)	0.34	84	90
MT 376	4747.386	Jcon(121)	0.08	82	90
	4610.632	Kcon(209)	0.34	81	60
	4612.522*	Kcon(209)	0.33	85	48
MT 390	4608.512	Kcon(209)	0.21	107	90
MT 403	4748.187	Jcon(121)	0.07	98	90
	4612.529	Kcon(209)	0.24	102	90
MT 417	3613.365	Jcon(112)	0.05	113	90
	3613.378	Hcon(157)	0.12	98	90
	3613.389	Kcon(209)	0.28	93	90
MT 421	5018.929	J PHARO	0.04	141	50
	5018.926	H PHARO	0.06	135	50
	5018.923	K_S PHARO	0.06	134	50
	4740.217	Kcon(209)	0.22	107	90
MT 429	4748.202	Jcon(121)	0.04	137	90
	4622.616	Kcon(209)	0.18	108	90
MT 431	3625.266	Jcon(112)	0.08	87	90
	3625.277	Hcon(157)	0.19	74	90
	3625.288	Kcon(209)	0.34	79	90
MT 448	4748.221	Jcon(121)	0.04	112	90
	4604.632	Kcon(209)	0.34	85	90
MT 455	4752.240	Jcon(121)	0.06	93	90

Table 3 *continued on next page*

Table 3 *(continued)*

Star Name	Date (JD – 2,450,000)	Filter Name	Strehl Ratio	FWHM (mas)	Number of Images
	4608.522	Kcon(209)	0.28	93	90
MT 457	3613.401	Jcon(112)	0.04	113	89
	3613.414	Hcon(157)	0.13	82	95
	3613.428	Kcon(209)	0.19	107	90
MT 462	4752.254	Jcon(121)	0.05	98	110
	4609.614	Kcon(209)	0.27	95	94
MT 465	3622.246	Jcon(112)	0.03	124	90
	3622.262	Hcon(157)	0.10	101	86
	3622.272	Kcon(209)	0.18	105	90
MT 470	4748.313	Jcon(121)	0.05	99	86
	4752.267*	Jcon(121)	0.05	99	90
	4624.592	Kcon(209)	0.16	106	90
MT 473	4798.187	Jcon(121)	0.04	100	90
	4611.592	Kcon(209)	0.24	99	90
MT 480	4611.602	Kcon(209)	0.22	106	90
MT 483	3625.369	Jcon(112)	0.05	108	90
	3625.381	Hcon(157)	0.15	89	80
	3625.393	Kcon(209)	0.23	104	90
MT 485	4611.610	Kcon(209)	0.24	101	90
MT 507	4624.605	Kcon(209)	0.17	108	90
MT 516	3632.362	Jcon(112)	0.02	151	90
	3632.380	Hcon(157)	0.07	82	90
	3632.390	Kcon(209)	0.15	81	90
MT 531	4752.286	Jcon(121)	0.05	98	99
	4612.619	Kcon(209)	0.19	108	91
MT 534	4605.612	Kcon(209)	0.19	110	90
MT 555	4613.606	Kcon(209)	0.19	109	90
MT 556	4752.223	Jcon(121)	0.05	100	111
	4613.616	Kcon(209)	0.21	106	90
MT 588	4594.622	Kcon(209)	0.25	97	90
MT 601	4752.194	Jcon(121)	0.05	103	90
	4607.635	Kcon(209)	0.22	104	90
MT 605	4752.206	Jcon(121)	0.03	151	90
	4613.626	Kcon(209)	0.15	148	90
MT 611	4817.194	Jcon(121)	0.04	111	90
	4605.623	Kcon(209)	0.22	102	90
MT 632	4751.184	Jcon(121)	0.02	119	90
	4614.548	Kcon(209)	0.18	106	90
MT 642	4753.220	Jcon(121)	0.04	107	90
	4617.583	Kcon(209)	0.21	103	90
MT 692	4618.600	Kcon(209)	0.17	112	78
MT 696	4617.594	Kcon(209)	0.19	106	90
MT 716	4740.204	Kcon(209)	0.22	107	90
MT 734	4753.231	Jcon(121)	0.04	109	90
	4614.621	Kcon(209)	0.43	82	17
	4618.510*	Kcon(209)	0.22	103	63

Table 3 *continued on next page*

Table 3 *(continued)*

Star Name	Date (JD – 2,450,000)	Filter Name	Strehl Ratio	FWHM (mas)	Number of Images
MT 736	4753.188	Jcon(121)	0.04	109	90
	4627.467	Kcon(209)	0.21	101	90
MT 745	4607.554	Kcon(209)	0.20	104	90
MT 771	4753.240	Jcon(121)	0.04	107	90
	4607.564	Kcon(209)	0.20	106	90
MT 793	4753.206	Jcon(121)	0.05	95	90
	4617.606	Kcon(209)	0.24	98	91
S 3	3626.319	Jcon(112)	0.03	124	87
	3626.361	Hcon(157)	0.07	117	90
	3626.370	Kcon(209)	0.15	115	90
S 5	4593.620	Kcon(209)	0.28	87	90
S 73	4593.629	Kcon(209)	0.19	101	90
WR 145	4740.194	Kcon(209)	0.26	97	90

References—^{C} Denotes that the combined image from both nights was used for analysis.
* Denotes which individual night was used for analysis.

The NIRI data were reduced using the tools provided as part of the Gemini reduction package in IRAF. With the images rotated, reduced, and the data quality robustly quantified through the various reduction steps, we used two different combining programs to co-add all of the frames. Most of the images were co-added using the IRAF tool IMCOADD to derive an average image taking into account the bad pixel mask. In the cases where IMCOADD failed (i.e., poor seeing, observations over multiple nights, or blended point spread functions), GEMCOMBINE was used with manual input of the central star pixel position. GEMCOMBINE produces a slightly different median image than the mean coadded IMCOADD, but the capability of allowing the user to define the pixel shifts makes the final co-added image better aligned than when IMCOADD fails. The final images from GEMCOMBINE and IMCOADD produce a slightly larger field of view than the $22'' \times 22''$ FOV of a single frame, but depending on the observing conditions (e.g., exposure time and observations spanning multiple nights) some fields can be larger than others. The PHARO data were reduced by debiasing, flat fielding, bad pixel correction, and background subtraction and then shift-and-added to create a single image.

We identified possible point sources by visually inspecting each frame using SAO Image display software. This proved more successful than automated methods due to the abundance of hot pixels from the IR detector confused as point sources. The faintest companions that we detect ($\Delta K \approx 9$ mag) have signals that are just above the threshold set by the readnoise of the camera and the number of coadded frames. We identified at least one source in addition to the main target in each K-band frame through visual inspection. After identifying each point source and estimating the approximate pixel position of its peak, we used SExtractor (Bertin & Arnouts 1996) to find each source and measure the centroid position and relative brightness. The positions were determined from the `XWIN_IMAGE` and the `YWIN_IMAGE` keywords in SExtractor. The relative flux returned by SExtractor is measured using the `FLUX_APER` parameter, which estimates the flux above the background within a circular aperture. We used nine aperture diameters on each star to create an enclosed energy curve. For close systems with blended point spread functions (PSFs) ($\rho \leq 0\farcs1$), we used a PSF deconvolution program, FITSTARS (ten Brummelaar et al. 1996, 2000), to measure the differential magnitude and separation.

3. RESULTS

We present the astrometric and photometric results for all the stars in Table 4 (given in full in the electronic version). The relative magnitudes and positions are determined with respect to the target stars. The columns of Table 4 give the main target name, the angular separation ρ and position angle θ (measured east from north) of the companion, its celestial coordinates, the magnitude difference and uncertainty in J, H, and K, the probability of chance alignment with a background field star P_{ca} (see section 4.2), the identification number in the UKIRT Infrared Deep Sky Survey (UKIDSS) (Lawrence et al. 2007), and notes indicating other names, correspondence in another field, or measurement by FITSTARS (FS). The first row for a given target corresponds to the bright central star, and succeeding rows list data where available for each detected companion star (arranged in order of increasing separation).

Table 4. Stars Detected in Sample

Field Name	ρ (arcsec)	θ (deg)	R.A. (HH:MM:SS)	Dec. (DD:MM:SS)	ΔJ (mag)	ΔH (mag)	ΔK (mag)	P_{ca}	UKIDSS Number	Notes
A 11	···	···	20:32:31.543	+41:14:08.21	···	···	···	···	438717749790	MT 267
	0.77	282.6	20:32:31.476	+41:14:08.38	···	···	4.71±0.03	0.000	···	
	1.28	175.6	20:32:31.552	+41:14:06.93	···	···	7.68±0.13	0.005	···	
	2.20	276.9	20:32:31.350	+41:14:08.48	···	···	4.17±0.02	0.002	438717693534	
	3.66	103.8	20:32:31.858	+41:14:07.34	···	···	9.00±0.31	0.068	···	
	5.26	195.1	20:32:31.422	+41:14:03.13	···	···	6.15±0.06	0.037	438717693527	
	5.89	179.4	20:32:31.549	+41:14:02.33	···	···	8.63±0.21	0.141	438717712064	
A 12	···	···	20:33:38.217	+40:41:06.40	···	···	···	···	438262710179	
	5.84	238.8	20:33:37.778	+40:41:03.38	···	···	7.65±0.12	0.063	438262710191	
	9.48	255.0	20:33:37.413	+40:41:03.94	···	···	8.61±0.22	0.236	438262710190	
A 15	···	···	20:31:36.906	+40:59:09.24	···	···	···	···	438261648600	
	5.20	79.5	20:31:37.358	+40:59:10.19	···	···	8.81±0.21	0.130	···	
	12.65	260.9	20:31:35.803	+40:59:07.23	···	···	7.34±0.10	0.358	438261648601	
	13.86	350.5	20:31:36.704	+40:59:22.91	···	···	6.22±0.06	0.263	438261648649	
A 18	···	···	20:30:07.881	+41:23:50.46	···	···	···	···	438773195713	
	4.17	190.0	20:30:07.817	+41:23:46.36	···	···	6.93±0.08	0.074	438773204014	
	4.44	98.9	20:30:08.271	+41:23:49.77	···	···	8.25±0.21	0.152	···	
	5.56	113.8	20:30:08.334	+41:23:48.21	···	···	7.27±0.10	0.148	438773195717	
	6.70	212.3	20:30:07.563	+41:23:44.80	···	···	9.06±0.26	0.427	438773195714	
	8.29	316.4	20:30:07.373	+41:23:56.46	···	···	8.15±0.17	0.421	438773195711	
	9.49	1.2	20:30:07.899	+41:23:59.95	···	···	7.16±0.17	0.358	···	
	9.59	73.6	20:30:08.699	+41:23:53.17	···	···	9.14±0.28	0.694	438773195731	
	9.67	356.1	20:30:07.823	+41:24:00.11	···	···	6.83±0.07	0.324	438773195712	
	9.83	17.0	20:30:08.137	+41:23:59.86	···	···	8.74±0.21	0.641	438773195621	
	12.61	241.3	20:30:06.898	+41:23:44.41	···	···	8.58±0.20	0.790	438773195434	
	12.65	52.3	20:30:08.772	+41:23:58.19	···	···	8.44±0.18	0.769	438773195741	
A 20	···	···	20:33:02.922	+40:47:25.44	···	···	···	···	438718069990	
	0.10	113.3	20:33:02.930	+40:47:25.40	···	···	1.75±0.31	0.000	···	FS
	2.55	240.6	20:33:02.726	+40:47:24.19	···	···	7.91±0.16	0.018	···	
	5.53	200.8	20:33:02.749	+40:47:20.28	···	···	8.57±0.24	0.104	438718079320	
	9.26	229.5	20:33:02.302	+40:47:19.43	···	···	6.99±0.09	0.142	438718069999	

Table 4 *continued on next page*

Table 4 *(continued)*

Field Name	ρ (arcsec)	θ (deg)	R.A. (HH:MM:SS)	Dec. (DD:MM:SS)	ΔJ (mag)	ΔH (mag)	ΔK (mag)	P_{ca}	UKIDSS Number	Notes
	15.65	340.5	20:33:02.462	+40:47:40.20	···	···	7.47±0.14	0.430	···	
A 23	···	···	20:30:39.709	+41:08:48.97	···	···	···	···	438773365458	
	8.72	346.0	20:30:39.523	+41:08:57.43	···	···	6.24±0.14	0.064	438773365476	
A 24	···	···	20:34:44.106	+40:51:58.50	···	···	···	···	438717927253	
	9.57	334.5	20:34:43.743	+40:52:07.13	···	···	9.14±0.30	0.530	438717939368	
	12.26	285.9	20:34:43.067	+40:52:01.86	···	···	8.26±0.17	0.554	438717927249	
A 25	···	···	20:32:38.436	+40:40:44.54	···	···	···	···	438262719910	
	7.52	62.9	20:32:39.025	+40:40:47.96	···	···	8.55±0.20	0.288	438262719912	
	8.13	129.7	20:32:38.986	+40:40:39.34	···	···	8.77±0.23	0.357	···	
	8.84	116.9	20:32:39.130	+40:40:40.54	···	···	8.26±0.17	0.334	438262727366	
	9.12	179.4	20:32:38.446	+40:40:35.43	···	···	7.58±0.11	0.268	438262719913	
	9.42	131.7	20:32:39.055	+40:40:38.28	···	···	5.44±0.04	0.114	438262719911	
	10.83	304.9	20:32:37.655	+40:40:50.73	···	···	8.39±0.19	0.478	···	
A 26	···	···	20:30:57.730	+41:09:57.57	···	···	···	···	438773367548	
	0.42	176.8	20:30:57.732	+41:09:57.16	···	···	2.13±0.45	0.000	···	FS
	5.01	247.0	20:30:57.322	+41:09:55.62	···	···	7.24±0.11	0.112	438773367551	
	7.48	113.4	20:30:58.338	+41:09:54.60	···	···	7.84±0.15	0.298	438773367549	
	9.50	312.6	20:30:57.110	+41:10:04.00	···	···	6.38±0.07	0.254	438773367547	
	9.59	255.9	20:30:56.907	+41:09:55.23	···	···	7.45±0.13	0.381	438773367546	
	11.30	82.1	20:30:58.721	+41:09:59.12	···	···	5.86±0.05	0.289	438773367623	
A 27	···	···	20:34:44.719	+40:51:46.56	···	···	···	···	438717927248	
	11.12	163.5	20:34:44.998	+40:51:35.90	···	···	7.06±0.10	0.152	438717927252	
	13.83	330.3	20:34:44.115	+40:51:58.57	1.72±0.01	···	···	···	438717927253	A 24
A 29	···	···	20:34:56.058	+40:38:18.06	···	···	···	···	438262442657	
	7.73	164.7	20:34:56.237	+40:38:10.61	···	···	8.65±0.27	0.221	438262442674	
A 32	···	···	20:32:30.331	+40:34:33.26	···	···	···	···	438262721119	
	3.28	153.2	20:32:30.461	+40:34:30.32	···	···	7.48±0.12	0.034	···	
	4.48	178.0	20:32:30.345	+40:34:28.78	···	···	8.74±0.25	0.107	···	
	6.33	84.1	20:32:30.884	+40:34:33.91	···	···	6.35±0.07	0.075	438262764414	
	7.44	64.6	20:32:30.921	+40:34:36.45	···	···	8.65±0.24	0.259	438262774411	
	9.17	261.4	20:32:29.536	+40:34:31.88	···	···	5.95±0.06	0.124	438262729347	
	11.47	31.3	20:32:30.853	+40:34:43.06	···	···	7.85±0.15	0.385	438262764411	
A 37	···	···	20:36:04.517	+40:56:12.98	···	···	···	···	438718034190	
	4.83	332.6	20:36:04.321	+40:56:17.27	···	···	9.18±0.33	0.198	···	

Table 4 *continued on next page*

Table 4 *(continued)*

Field Name	ρ (arcsec)	θ (deg)	R.A. (HH:MM:SS)	Dec. (DD:MM:SS)	ΔJ (mag)	ΔH (mag)	ΔK (mag)	P_{ca}	UKIDSS Number	Notes
	5.36	245.2	20:36:04.088	+40:56:10.73	···	···	8.64±0.22	0.188	438718040280	
	6.61	175.1	20:36:04.567	+40:56:06.39	···	···	8.87±0.27	0.299	438718041369	
	7.48	113.4	20:36:05.123	+40:56:10.01	···	···	7.43±0.12	0.202	438718034192	
	14.02	328.8	20:36:03.877	+40:56:24.98	···	···	7.49±0.12	0.557	438718034162	
A 38	···	···	20:32:34.868	+40:56:17.43	···	···	···	···	438718075096	
	0.93	118.0	20:32:34.940	+40:56:17.00	···	···	5.63±0.05	0.002	···	
	2.38	25.3	20:32:34.958	+40:56:19.58	···	···	5.94±0.05	0.018	···	
	3.47	326.4	20:32:34.698	+40:56:20.32	···	···	8.32±0.17	0.108	···	
	4.42	133.8	20:32:35.149	+40:56:14.37	···	···	8.75±0.22	0.205	···	
	7.55	151.4	20:32:35.187	+40:56:10.80	···	···	7.48±0.13	0.303	438718075097	
	8.09	9.7	20:32:34.988	+40:56:25.40	···	···	8.45±0.19	0.485	438718081653	
	8.60	339.3	20:32:34.600	+40:56:25.47	···	···	2.61±0.01	0.031	438718075099	
	10.58	162.0	20:32:35.156	+40:56:07.37	···	···	6.35±0.06	0.338	438718074935	
	11.40	184.0	20:32:34.798	+40:56:06.05	···	···	6.20±0.09	0.364	438718074994	
	11.75	315.6	20:32:34.142	+40:56:25.83	···	···	7.17±0.10	0.528	438718075098	
	13.54	64.3	20:32:35.945	+40:56:23.31	···	···	7.67±0.13	0.720	438718074801	
A 41	···	···	20:31:08.381	+42:02:42.28	···	···	···	···	438768916027	
	0.34	258.3	20:31:08.351	+42:02:42.21	3.84±1.47	···	4.90±2.40	0.000	···	FS
	4.22	220.6	20:31:08.135	+42:02:39.08	9.17±0.30	···	8.39±0.24	0.080	···	
A 46	···	···	20:31:00.195	+40:49:49.74	···	···	···	···	438773477531	
	2.56	270.4	20:30:59.969	+40:49:49.75	···	···	7.96±0.18	0.036	···	
	8.28	334.8	20:30:59.884	+40:49:57.23	···	···	4.74±0.04	0.075	438773477533	
	8.44	92.6	20:31:00.938	+40:49:49.36	···	···	7.17±0.13	0.237	438773477534	
B 17	···	···	20:30:27.302	+41:13:25.31	···	···	···	···	438773119033	
	4.88	106.7	20:30:27.716	+41:13:23.91	···	···	6.91±0.10	0.044	438773119044	
	8.34	286.4	20:30:26.592	+41:13:27.66	···	···	6.48±0.07	0.098	438773119042	
	9.75	107.8	20:30:28.124	+41:13:22.33	···	···	7.24±0.13	0.191	438773119040	
	10.57	13.5	20:30:27.521	+41:13:35.59	···	···	8.24±0.19	0.315	438773119039	
MT 5	···	···	20:30:39.816	+41:36:50.72	···	···	···	···	438768151198	
	0.32	90.9	20:30:39.845	+41:36:50.72	2.59±0.67	···	2.60±0.67	0.000	···	FS
	2.64	335.6	20:30:39.719	+41:36:53.13	8.01±0.11	···	7.27±0.06	0.035	···	
	6.00	341.5	20:30:39.646	+41:36:56.42	7.48±0.08	···	7.65±0.07	0.197	438768151202	
	6.99	167.8	20:30:39.948	+41:36:43.89	···	···	8.92±0.21	0.424	438768163606	
	7.75	336.6	20:30:39.542	+41:36:57.84	···	···	9.26±0.17	0.551	···	

Table 4 *continued on next page*

Table 4 *(continued)*

Field Name	ρ (arcsec)	θ (deg)	R.A. (HH:MM:SS)	Dec. (DD:MM:SS)	ΔJ (mag)	ΔH (mag)	ΔK (mag)	P_{ca}	UKIDSS Number	Notes
	8.20	20.0	20:30:40.067	+41:36:58.43	···	···	8.41±0.11	0.447	438768151200	
	9.00	158.2	20:30:40.114	+41:36:42.36	8.16±0.11	···	5.95±0.04	0.209	438768151199	
	9.23	284.0	20:30:39.018	+41:36:52.96	8.00±0.09	···	7.12±0.06	0.330	438768151219	
	10.06	43.5	20:30:40.434	+41:36:58.03	8.13±0.10	···	6.74±0.05	0.327	438768151197	
	10.09	118.1	20:30:40.610	+41:36:45.98	···	···	7.58±0.08	0.451	438768150989	
	10.23	14.2	20:30:40.040	+41:37:00.64	7.38±0.07	···	7.05±0.06	0.378	438768151201	
	10.34	104.3	20:30:40.710	+41:36:48.17	···	···	8.90±0.21	0.697	438768150969	
	11.97	77.3	20:30:40.858	+41:36:53.36	···	···	8.49±0.11	0.731	438768150952	
	13.40	1.6	20:30:39.850	+41:37:04.12	6.57±0.05	···	···	···	438768151113	
	13.77	281.1	20:30:38.611	+41:36:53.38	7.62±0.08	···	···	···	438768151281	
MT 59	···	···	20:31:10.552	+41:31:53.54	···	···	···	···	438768179217	CygOB2-1
	1.17	342.0	20:31:10.519	+41:31:54.66	2.12±0.01	···	2.61±0.01	0.000	···	
	6.34	152.0	20:31:10.817	+41:31:47.95	···	···	8.57±0.28	0.214	···	
MT 70	···	···	20:31:18.330	+41:21:21.66	···	···	···	···	438773128806	
	4.36	214.8	20:31:18.109	+41:21:18.08	4.53±0.02	···	4.57±0.03	0.018	438773128810	
	6.57	185.4	20:31:18.275	+41:21:15.12	···	···	7.51±0.14	0.170	438717709448	
	10.70	100.7	20:31:19.264	+41:21:19.68	···	···	7.21±0.17	0.349	438717700400	
	11.09	115.9	20:31:19.216	+41:21:16.82	···	···	7.33±0.13	0.385	438717700402	
	11.37	233.9	20:31:17.514	+41:21:14.97	···	···	6.98±0.20	0.359	438773128431	
	12.40	274.0	20:31:17.231	+41:21:22.52	···	···	7.24±0.13	0.441	···	
	12.66	275.2	20:31:17.210	+41:21:22.80	···	···	7.67±0.16	0.526	···	
	13.33	271.9	20:31:17.147	+41:21:22.11	···	···	5.85±0.06	0.314	438773128391	
MT 83	···	···	20:31:22.039	+41:31:28.41	···	···	···	···	438768177042	CygOB2-2
	3.90	115.5	20:31:22.352	+41:31:26.74	6.16±0.05	···	5.74±0.06	0.028	438768177049	
	5.99	30.4	20:31:22.309	+41:31:33.58	7.40±0.11	···	6.88±0.10	0.107	438768177048	
MT 138	···	···	20:31:45.402	+41:18:26.75	···	···	···	···	438717697466	
	1.31	37.6	20:31:45.473	+41:18:27.78	2.47±0.01	···	3.04±0.02	0.001	438717708212	
	6.42	280.5	20:31:44.842	+41:18:27.92	···	···	6.85±0.14	0.106	···	
	6.44	282.0	20:31:44.844	+41:18:28.08	6.12±0.05	···	5.89±0.06	0.068	438717697477	
	6.93	337.7	20:31:45.169	+41:18:33.16	6.46±0.06	···	5.68±0.06	0.069	438717697475	
	7.99	359.6	20:31:45.397	+41:18:34.73	8.63±0.24	···	7.11±0.12	0.175	438717697476	
	9.00	225.7	20:31:44.831	+41:18:20.46	···	···	8.26±0.24	0.328	438717697473	
	11.86	347.6	20:31:45.177	+41:18:38.33	···	···	8.33±0.26	0.510	438717697470	
	13.03	183.1	20:31:45.340	+41:18:13.74	6.14±0.06	···	6.09±0.09	0.272	438717697472	

Table 4 *continued on next page*

Table 4 *(continued)*

Field Name	ρ (arcsec)	θ (deg)	R.A. (HH:MM:SS)	Dec. (DD:MM:SS)	ΔJ (mag)	ΔH (mag)	ΔK (mag)	P_{ca}	UKIDSS Number	Notes
MT 140	···	···	20:31:46.008	+41:17:27.08	···	···	···	···	438717712804	Not a member of Cyg OB2
	3.53	22.2	20:31:46.126	+41:17:30.34	···	···	7.11±0.11	0.050	···	
	5.02	146.4	20:31:46.255	+41:17:22.90	···	···	5.90±0.06	0.062	438717696514	
	6.64	3.6	20:31:46.046	+41:17:33.71	···	···	4.50±0.03	0.048	438717696513	
	8.29	117.4	20:31:46.661	+41:17:23.26	···	···	6.17±0.07	0.177	438717696512	
	10.65	93.7	20:31:46.952	+41:17:26.39	···	···	7.47±0.13	0.426	438717696511	
	12.63	47.2	20:31:46.831	+41:17:35.65	···	···	7.85±0.16	0.610	438717696507	
	13.71	223.8	20:31:45.166	+41:17:17.19	···	···	7.74±0.15	0.650	438717696185	
	15.79	254.9	20:31:44.656	+41:17:22.96	···	···	5.80±0.06	0.453	···	
MT 145	···	···	20:31:49.659	+41:28:26.52	···	···	···	···	438768171558	CygOB2-20
	2.89	275.8	20:31:49.403	+41:28:26.81	7.43±0.16	···	6.82±0.09	0.039	···	
	2.99	327.6	20:31:49.516	+41:28:29.04	7.23±0.15	···	5.82±0.06	0.027	···	
	3.48	62.7	20:31:49.934	+41:28:28.11	6.90±0.13	···	6.74±0.09	0.054	···	
	4.81	176.6	20:31:49.684	+41:28:21.72	8.09±0.25	···	7.74±0.15	0.158	438768182713	
	5.43	112.4	20:31:50.105	+41:28:24.45	···	···	8.61±0.30	0.284	438768182712	
	5.87	92.2	20:31:50.181	+41:28:26.29	···	···	8.99±0.35	0.375	···	
	8.29	147.7	20:31:50.053	+41:28:19.51	···	···	8.36±0.22	0.499	438768171560	
	9.51	294.9	20:31:48.891	+41:28:30.52	6.14±0.08	···	5.70±0.05	0.235	438768171559	
	9.52	340.6	20:31:49.378	+41:28:35.50	···	···	8.72±0.32	0.662	438768182661	
	9.61	7.0	20:31:49.763	+41:28:36.06	···	···	8.44±0.23	0.619	438768171303	
	9.62	104.6	20:31:50.487	+41:28:24.09	···	···	7.14±0.11	0.402	438768171557	
	11.96	281.4	20:31:48.615	+41:28:28.88	5.22±0.05	···	5.19±0.05	0.289	438768171561	
	12.26	6.6	20:31:49.783	+41:28:38.70	···	···	7.38±0.13	0.608	438768171297	
MT 213	···	···	20:32:13.129	+41:27:24.36	···	···	···	···	438768166682	CygOB2-4B
	7.16	38.3	20:32:13.524	+41:27:29.98	1.60±0.01	···	2.49±0.01	0.028	438768166685	MT 215, CygOB2-4C
	11.22	354.1	20:32:13.026	+41:27:35.52	···	···	7.80±0.22	0.696	···	
	11.78	354.0	20:32:13.020	+41:27:36.08	···	···	6.21±0.13	0.454	···	
	12.00	352.7	20:32:12.994	+41:27:36.27	···	···	6.65±0.14	0.541	···	
	12.98	161.0	20:32:13.505	+41:27:12.09	4.92±0.04	···	4.33±0.04	0.276	438768180689	see MT 217
	14.66	147.5	20:32:13.829	+41:27:12.00	-1.94±0.01	···	···	···	438768180687	MT 217, CygOB2-4A
MT 217	···	···	20:32:13.830	+41:27:12.03	···	···	···	···	438768180687	CygOB2-4A
	3.56	270.6	20:32:13.513	+41:27:12.07	6.30±0.06	···	4.87±0.04	0.009	438768180689	see MT 213
	5.51	272.4	20:32:13.341	+41:27:12.26	···	···	8.19±0.23	0.125	···	
	6.05	269.5	20:32:13.292	+41:27:11.98	···	···	7.36±0.24	0.108	···	

Table 4 *continued on next page*

Table 4 *(continued)*

Field Name	ρ (arcsec)	θ (deg)	R.A. (HH:MM:SS)	Dec. (DD:MM:SS)	ΔJ (mag)	ΔH (mag)	ΔK (mag)	P_{ca}	UKIDSS Number	Notes
	8.46	270.6	20:32:13.077	+41:27:12.11	···	···	7.37±0.15	0.201	438768166684	
	14.57	327.8	20:32:13.139	+41:27:24.36	1.94±0.01	···	0.86±0.01	0.005	438768166682	MT 213, CygOB2-4B
MT 227	···	···	20:32:16.565	+41:25:35.71	···	···	···	···	438768165898	CygOB2-14
	3.85	129.3	20:32:16.829	+41:25:33.27	···	···	5.10±0.05	0.026	438768165903	
	5.24	172.1	20:32:16.629	+41:25:30.52	···	···	7.21±0.13	0.119	438768318285	
	6.23	349.8	20:32:16.466	+41:25:41.84	···	···	6.68±0.19	0.131	438717714184	
	9.00	77.1	20:32:17.345	+41:25:37.72	···	···	7.76±0.18	0.387	···	
	11.85	350.7	20:32:16.394	+41:25:47.40	···	···	5.36±0.05	0.252	438768165900	
	13.69	307.7	20:32:15.602	+41:25:44.09	···	···	6.66±0.11	0.490	438768165972	
MT 250	···	···	20:32:26.084	+41:29:39.36	···	···	···	···	438768309130	
	1.71	250.8	20:32:25.940	+41:29:38.80	5.20±0.04	···	5.45±0.05	0.014	···	
	3.58	350.7	20:32:26.032	+41:29:42.89	···	···	8.21±0.20	0.207	···	
	5.27	248.3	20:32:25.648	+41:29:37.42	···	···	6.66±0.09	0.211	438768309134	
	5.78	210.0	20:32:25.826	+41:29:34.36	···	···	8.09±0.19	0.435	438768319273	
	6.52	243.5	20:32:25.564	+41:29:36.45	···	···	8.24±0.21	0.542	···	
	6.87	200.1	20:32:25.873	+41:29:32.91	···	···	8.72±0.32	0.665	···	
	7.04	241.8	20:32:25.532	+41:29:36.04	···	···	6.11±0.07	0.276	438768309135	
	7.37	201.8	20:32:25.840	+41:29:32.51	···	···	6.22±0.07	0.312	438768309166	
	7.74	277.8	20:32:25.402	+41:29:40.41	5.31±0.05	···	4.63±0.04	0.180	438768309131	
	8.08	340.0	20:32:25.838	+41:29:46.95	···	···	8.12±0.19	0.677	438768308897	
	9.01	237.4	20:32:25.408	+41:29:34.51	···	···	8.60±0.27	0.831	···	
	9.55	236.5	20:32:25.375	+41:29:34.09	···	···	6.26±0.07	0.472	438768309133	
	9.72	14.1	20:32:26.295	+41:29:48.79	···	···	5.42±0.05	0.356	···	
	9.89	253.1	20:32:25.242	+41:29:36.49	···	···	6.86±0.18	0.601	438768316954	
	9.89	156.6	20:32:26.433	+41:29:30.29	···	···	7.41±0.13	0.699	438768316979	
	9.98	347.6	20:32:25.892	+41:29:49.11	···	···	6.68±0.09	0.575	438768308890	
	10.35	350.1	20:32:25.926	+41:29:49.56	···	···	8.02±0.18	0.829	···	
	10.37	8.6	20:32:26.221	+41:29:49.62	3.62±0.02	···	2.88±0.02	0.142	438768308889	
	10.59	277.4	20:32:25.149	+41:29:40.72	···	···	5.05±0.04	0.353	438768309132	
	11.03	76.7	20:32:27.039	+41:29:41.90	3.32±0.02	···	2.59±0.01	0.130	438768309055	
MT 258	···	···	20:32:27.663	+41:26:22.08	···	···	···	···	438768312775	CygOB2-15
	1.57	192.5	20:32:27.633	+41:26:20.56	4.40±0.02	···	5.46±0.05	0.005	···	
	1.96	320.3	20:32:27.552	+41:26:23.59	6.82±0.09	···	6.19±0.08	0.011	···	
	3.40	227.4	20:32:27.441	+41:26:19.79	···	···	6.57±0.15	0.037	···	

Table 4 *continued on next page*

Table 4 *(continued)*

Field Name	ρ (arcsec)	θ (deg)	R.A. (HH:MM:SS)	Dec. (DD:MM:SS)	ΔJ (mag)	ΔH (mag)	ΔK (mag)	P_{ca}	UKIDSS Number	Notes
	6.75	157.2	20:32:27.896	+41:26:15.87	···	···	7.88±0.20	0.236	438768319605	
	7.58	40.7	20:32:28.103	+41:26:27.83	···	···	7.73±0.21	0.270	438768312779	
	7.82	169.0	20:32:27.796	+41:26:14.40	6.32±0.06	···	5.45±0.06	0.115	438768312781	
	8.00	293.1	20:32:27.008	+41:26:25.22	7.43±0.12	···	6.77±0.11	0.202	438768312777	
	9.92	43.7	20:32:28.272	+41:26:29.26	···	···	8.03±0.23	0.465	438768312776	
	10.07	25.8	20:32:28.053	+41:26:31.15	···	···	8.23±0.26	0.508	438768312475	
	10.07	232.0	20:32:26.958	+41:26:15.88	···	···	7.54±0.17	0.398	438768312774	
	11.74	209.6	20:32:27.148	+41:26:11.87	···	···	7.95±0.22	0.569	438768312792	
	12.65	236.4	20:32:26.726	+41:26:15.09	···	···	7.71±0.19	0.581	438768312773	
	13.96	305.2	20:32:26.649	+41:26:30.14	···	···	7.32±0.16	0.584	438768312505	
	15.00	313.7	20:32:26.699	+41:26:32.46	···	···	7.87±0.22	0.733	···	
	15.16	322.7	20:32:26.846	+41:26:34.13	5.37±0.03	···	5.21±0.05	0.332	···	
MT 259	···	···	20:32:27.744	+41:28:52.28	···	···	···	···	438768310062	CygOB2-21
	3.63	181.2	20:32:27.737	+41:28:48.66	···	···	6.87±0.10	0.066	438768319357	
	3.90	69.7	20:32:28.070	+41:28:53.64	···	···	8.14±0.20	0.136	···	
	4.52	82.3	20:32:28.142	+41:28:52.89	···	···	8.04±0.19	0.171	···	
	6.23	136.6	20:32:28.125	+41:28:47.75	···	···	7.23±0.13	0.213	438768310068	
	6.27	171.8	20:32:27.824	+41:28:46.08	···	···	5.09±0.05	0.091	438768310069	
	6.88	352.1	20:32:27.659	+41:28:59.09	···	···	7.33±0.13	0.265	438768310067	
	7.48	222.0	20:32:27.298	+41:28:46.73	···	···	5.52±0.05	0.150	438768310065	
	7.54	267.3	20:32:27.074	+41:28:51.93	···	···	5.81±0.06	0.169	438768310064	
	7.72	355.2	20:32:27.686	+41:28:59.98	···	···	7.86±0.18	0.394	···	
	8.72	119.2	20:32:28.422	+41:28:48.03	···	···	7.72±0.17	0.449	438768309963	
	9.15	180.7	20:32:27.734	+41:28:43.13	···	···	6.47±0.09	0.301	···	
	9.19	181.8	20:32:27.719	+41:28:43.09	···	···	6.30±0.08	0.283	438768310066	
	10.44	297.0	20:32:26.916	+41:28:57.02	···	···	5.97±0.07	0.313	438768309846	
	11.17	347.7	20:32:27.532	+41:29:03.19	···	···	7.83±0.24	0.644	438768309717	
	14.05	28.2	20:32:28.334	+41:29:04.67	···	···	5.78±0.06	0.470	438768309703	
MT 299	···	···	20:32:38.579	+41:25:13.75	···	···	···	···	438717763494	CygOB2-16
	1.08	234.7	20:32:38.500	+41:25:13.13	5.06±0.02	···	5.80±0.08	0.002	···	
	2.34	304.5	20:32:38.407	+41:25:15.08	8.57±0.20	···	7.86±0.15	0.027	···	
	5.75	205.7	20:32:38.356	+41:25:08.57	7.86±0.14	···	7.36±0.12	0.122	438717763499	
	7.78	25.0	20:32:38.871	+41:25:20.80	2.38±0.01	···	2.36±0.01	0.020	438717763501	
	8.56	83.7	20:32:39.335	+41:25:14.69	8.44±0.21	···	7.22±0.11	0.238	438717763497	MT 300

Table 4 *continued on next page*

Table 4 *(continued)*

Field Name	ρ (arcsec)	θ (deg)	R.A. (HH:MM:SS)	Dec. (DD:MM:SS)	ΔJ (mag)	ΔH (mag)	ΔK (mag)	P_{ca}	UKIDSS Number	Notes
	10.74	9.1	20:32:38.729	+41:25:24.36	···	···	5.84±0.06	0.213	438717763500	
MT 304	···	···	20:32:40.962	+41:14:29.16	···	···	···	···	438717750871	CygOB2-12
	1.06	270.4	20:32:40.868	+41:14:29.16	5.82±0.06	···	4.16±0.02	0.000	···	
MT 317	···	···	20:32:45.456	+41:25:37.43	···	···	···	···	438717769175	CygOB2-6
	8.31	278.9	20:32:44.726	+41:25:38.72	···	···	6.73±0.09	0.174	438717763871	
	8.33	20.0	20:32:45.710	+41:25:45.25	···	···	7.49±0.14	0.226	438717763870	
	13.22	308.9	20:32:44.541	+41:25:45.73	···	···	5.46±0.05	0.221	438717763865	
MT 339	···	···	20:32:50.021	+41:23:44.68	···	···	···	···	438717761231	CygOB2-17
	1.55	169.4	20:32:50.046	+41:23:43.16	···	···	8.70±0.22	0.021	···	
	2.51	29.8	20:32:50.132	+41:23:46.86	···	···	8.77±0.23	0.055	···	
	3.93	330.2	20:32:49.848	+41:23:48.09	···	···	8.68±0.22	0.124	···	
	5.65	74.6	20:32:50.506	+41:23:46.18	···	···	7.10±0.10	0.119	438717761235	
	5.66	161.6	20:32:50.180	+41:23:39.31	···	···	7.13±0.10	0.121	438717761234	
	8.08	125.9	20:32:50.603	+41:23:39.95	···	···	8.09±0.16	0.342	438717761232	
	8.79	265.5	20:32:49.242	+41:23:43.98	···	···	8.69±0.29	0.485	438717761233	
	10.84	172.9	20:32:50.140	+41:23:33.92	···	···	6.20±0.11	0.280	···	
	10.86	15.1	20:32:50.273	+41:23:55.16	···	···	7.07±0.10	0.369	438717761298	
	12.80	138.2	20:32:50.780	+41:23:35.14	···	···	6.18±0.06	0.366	438717760854	
MT 376	···	···	20:32:59.190	+41:24:25.47	···	···	···	···	438717762201	
	3.13	156.8	20:32:59.300	+41:24:22.59	7.12±0.15	···	6.39±0.08	0.033	438717768710	
	5.17	276.4	20:32:58.734	+41:24:26.04	···	···	8.47±0.24	0.215	438717770632	
	7.93	282.6	20:32:58.503	+41:24:27.19	···	···	8.47±0.29	0.435	438717762204	
	8.20	8.2	20:32:59.294	+41:24:33.58	···	···	8.13±0.20	0.404	438717762203	
	9.17	223.8	20:32:58.627	+41:24:18.84	4.58±0.03	···	4.63±0.04	0.118	438717762205	
	10.28	256.5	20:32:58.302	+41:24:23.07	···	···	8.30±0.22	0.586	438717761917	
	10.92	111.4	20:33:00.094	+41:24:21.48	···	···	7.16±0.12	0.436	438717761899	
MT 390	···	···	20:33:02.922	+41:17:43.13	···	···	···	···	438717753790	
	2.93	157.8	20:33:03.020	+41:17:40.42	···	···	7.46±0.13	0.038	···	
	5.15	191.1	20:33:02.833	+41:17:38.08	···	···	7.46±0.14	0.112	438717753797	
	6.51	229.4	20:33:02.483	+41:17:38.89	···	···	5.78±0.06	0.089	438717753796	
	6.74	71.0	20:33:03.487	+41:17:45.33	···	···	8.96±0.36	0.344	438717753795	
	9.07	27.1	20:33:03.288	+41:17:51.20	···	···	7.84±0.20	0.358	438717753794	
	10.11	44.3	20:33:03.548	+41:17:50.36	···	···	8.49±0.26	0.530	438717753792	
	11.65	254.1	20:33:01.927	+41:17:39.94	···	···	5.76±0.06	0.255	438717753555	

Table 4 *continued on next page*

Table 4 *(continued)*

Field Name	ρ (arcsec)	θ (deg)	R.A. (HH:MM:SS)	Dec. (DD:MM:SS)	ΔJ (mag)	ΔH (mag)	ΔK (mag)	P_{ca}	UKIDSS Number	Notes
	12.85	120.1	20:33:03.908	+41:17:36.68	···	···	4.65±0.04	0.166	438717753514	
	14.75	204.7	20:33:02.374	+41:17:29.74	···	···	7.14±0.13	0.566	438717753359	
MT 403	···	···	20:33:05.268	+41:43:36.79	···	···	···	···	438768537709	
	1.83	167.4	20:33:05.304	+41:43:35.01	4.22±0.03	···	4.12±0.02	0.004	···	
	7.44	31.7	20:33:05.618	+41:43:43.13	6.98±0.12	···	6.31±0.07	0.186	438768537712	
	8.04	237.5	20:33:04.663	+41:43:32.47	···	···	8.27±0.20	0.461	438768537710	
	8.24	159.0	20:33:05.533	+41:43:29.10	8.01±0.21	···	7.39±0.12	0.345	···	
	8.25	157.6	20:33:05.550	+41:43:29.17	7.37±0.14	···	6.39±0.07	0.230	438768537713	
	10.62	287.1	20:33:04.361	+41:43:39.91	···	···	6.89±0.21	0.424	438768537552	
	11.52	113.7	20:33:06.210	+41:43:32.16	6.78±0.11	···	6.04±0.06	0.359	438768537687	
	12.60	85.7	20:33:06.391	+41:43:37.74	7.14±0.13	···	6.94±0.11	0.549	438768537589	
	12.66	122.7	20:33:06.219	+41:43:29.95	6.62±0.10	···	6.22±0.07	0.438	438768537686	
	14.89	347.4	20:33:04.979	+41:43:51.33	6.54±0.09	···	···	···	···	
MT 417	···	···	20:33:08.799	+41:13:18.21	···	···	···	···	438717748816	CygOB2-22A
	1.53	146.3	20:33:08.874	+41:13:16.94	0.66±0.01	0.68±0.01	0.80±0.01	0.000	438717769433	CygOB2-22Ba
	1.71	150.5	20:33:08.873	+41:13:16.72	3.01±0.02	2.95±0.01	3.06±0.02	0.000	···	CygOB2-22Bb
	5.17	112.6	20:33:09.222	+41:13:16.22	···	7.57±0.18	6.13±0.18	0.026	438717769429	see MT 421
	6.29	147.5	20:33:09.098	+41:13:12.91	···	8.06±0.21	7.50±0.21	0.086	438717764491	see MT 421
	7.58	76.3	20:33:09.451	+41:13:20.01	···	7.40±0.15	7.65±0.23	0.132	438717748832	
	9.29	9.1	20:33:08.928	+41:13:27.38	···	7.68±0.18	7.51±0.22	0.179	438717748824	
	9.37	201.8	20:33:08.490	+41:13:09.51	···	7.05±0.12	6.46±0.13	0.103	438717748822	see MT 421
	9.92	345.2	20:33:08.574	+41:13:27.80	···	7.23±0.15	6.93±0.16	0.153	438717748818	
	10.77	157.6	20:33:09.162	+41:13:08.25	···	6.62±0.09	6.56±0.13	0.143	438717748815	see MT 421
	12.60	311.2	20:33:07.959	+41:13:26.51	4.43±0.04	4.10±0.02	···	···	438717748823	
	13.16	12.7	20:33:09.054	+41:13:31.05	···	7.42±0.17	···	···	438717748977	
MT 421	···	···	20:33:09.603	+41:13:00.55	···	···	···	···	438717748838	
	2.62	205.0	20:33:09.505	+41:12:58.18	···	···	7.01±0.07	0.024	···	
	2.83	218.4	20:33:09.447	+41:12:58.34	1.77±0.01	1.75±0.01	1.73±0.01	0.001	438717748827	MT 420
	3.67	307.6	20:33:09.345	+41:13:02.80	···	···	9.33±0.40	0.132	···	
	3.85	32.7	20:33:09.787	+41:13:03.79	4.06±0.01	3.98±0.01	3.91±0.01	0.009	438717748836	
	4.10	291.5	20:33:09.265	+41:13:02.05	6.20±0.06	5.50±0.02	5.20±0.02	0.025	438717748835	
	4.41	13.5	20:33:09.695	+41:13:04.83	···	6.67±0.05	6.45±0.05	0.054	···	
	4.54	207.1	20:33:09.419	+41:12:56.51	3.17±0.01	3.17±0.01	3.17±0.01	0.008	438717748837	
	5.36	79.0	20:33:10.069	+41:13:01.58	7.28±0.14	6.51±0.04	6.33±0.04	0.075	438717748831	

Table 4 *continued on next page*

Table 4 *(continued)*

Field Name	ρ (arcsec)	θ (deg)	R.A. (HH:MM:SS)	Dec. (DD:MM:SS)	ΔJ (mag)	ΔH (mag)	ΔK (mag)	P_{ca}	UKIDSS Number	Notes
	5.80	146.5	20:33:09.886	+41:12:55.72	···	···	8.54±0.18	0.215	438717764487	
	6.56	313.4	20:33:09.181	+41:13:05.07	6.60±0.09	6.35±0.04	6.15±0.04	0.102	438717748825	
	6.68	220.0	20:33:09.222	+41:12:55.43	···	7.20±0.07	6.89±0.06	0.139	···	
	7.46	59.7	20:33:10.174	+41:13:04.31	···	7.86±0.13	8.46±0.17	0.319	438717764488	
	7.71	0.1	20:33:09.605	+41:13:08.26	6.75±0.09	6.20±0.04	5.84±0.03	0.119	438717748828	
	7.86	102.3	20:33:10.284	+41:12:58.88	4.47±0.02	4.35±0.01	4.28±0.01	0.046	438717748826	
	8.15	273.2	20:33:08.881	+41:13:01.01	···	6.52±0.05	6.57±0.06	0.179	438717748820	
	8.24	213.4	20:33:09.200	+41:12:53.67	2.52±0.01	2.44±0.01	2.38±0.01	0.023	438717748834	
	8.52	196.5	20:33:09.388	+41:12:52.38	7.73±0.19	6.84±0.05	6.72±0.05	0.204	···	
	9.35	22.8	20:33:09.924	+41:13:09.17	···	···	7.00±0.13	0.263	···	
	9.57	251.6	20:33:08.798	+41:12:57.53	5.10±0.03	4.58±0.01	4.43±0.01	0.076	438717748819	
	9.73	326.6	20:33:09.128	+41:13:08.67	5.99±0.05	5.26±0.02	5.02±0.02	0.118	438717748815	see MT 417
	9.73	253.6	20:33:08.777	+41:12:57.79	···	6.38±0.04	6.15±0.04	0.211	···	
	9.77	133.5	20:33:10.231	+41:12:53.82	···	8.38±0.15	8.15±0.14	0.433	438717748787	
	9.78	24.0	20:33:09.957	+41:13:09.48	6.30±0.07	5.87±0.03	5.56±0.03	0.162	···	
	9.81	255.8	20:33:08.760	+41:12:58.15	···	···	6.33±0.21	0.230	···	
	9.82	171.9	20:33:09.726	+41:12:50.83	6.63±0.08	6.04±0.03	5.69±0.03	0.173	438717748811	
	10.02	333.4	20:33:09.205	+41:13:09.51	6.77±0.10	6.55±0.05	6.15±0.04	0.222	···	
	10.05	198.0	20:33:09.328	+41:12:51.00	5.54±0.04	5.01±0.02	4.98±0.02	0.122	438717748833	
	10.08	140.7	20:33:10.169	+41:12:52.75	···	7.53±0.08	6.29±0.04	0.238	438717769340	
	10.09	274.6	20:33:08.712	+41:13:01.36	6.37±0.07	6.03±0.03	5.81±0.03	0.192	438717748821	
	10.15	198.9	20:33:09.312	+41:12:50.95	···	···	6.32±0.05	0.243	···	
	10.45	59.0	20:33:10.397	+41:13:05.93	5.41±0.03	5.54±0.02	5.66±0.03	0.191	438717748830	MT 426
	10.95	10.8	20:33:09.785	+41:13:11.30	···	9.17±0.28	8.99±0.26	0.658	···	
	11.21	184.5	20:33:09.525	+41:12:49.38	···	8.14±0.13	7.86±0.22	0.477	438717748799	
	11.21	31.6	20:33:10.124	+41:13:10.09	0.58±0.01	0.57±0.01	0.59±0.01	0.004	438717748798	MT 425
	11.70	359.5	20:33:09.593	+41:13:12.25	···	8.14±0.13	7.65±0.09	0.471	438717748812	
	11.96	290.8	20:33:08.612	+41:13:04.80	···	6.31±0.04	6.61±0.06	0.350	438717748352	
	12.76	166.9	20:33:09.859	+41:12:48.12	···	···	6.09±0.09	0.326	438717748054	
	12.89	337.9	20:33:09.174	+41:13:12.50	···	8.50±0.17	8.18±0.14	0.633	···	
	13.10	299.8	20:33:08.596	+41:13:07.05	···	7.83±0.10	7.78±0.10	0.573	438717748788	
	13.17	266.0	20:33:08.439	+41:12:59.63	···	8.55±0.17	8.03±0.13	0.622	438717748233	
	13.38	277.8	20:33:08.429	+41:13:02.35	···	8.84±0.22	8.30±0.16	0.682	438717748298	
	13.57	239.6	20:33:08.565	+41:12:53.69	5.40±0.03	5.17±0.02	5.12±0.02	0.232	438717748786	

Table 4 *continued on next page*

Table 4 *(continued)*

Field Name	ρ (arcsec)	θ (deg)	R.A. (HH:MM:SS)	Dec. (DD:MM:SS)	ΔJ (mag)	ΔH (mag)	ΔK (mag)	P_{ca}	UKIDSS Number	Notes
	14.12	334.6	20:33:09.066	+41:13:13.31	···	6.46±0.04	5.96±0.04	0.364	438717764491	see MT 417
	15.97	305.3	20:33:08.449	+41:13:09.76	6.87±0.10	5.41±0.02	4.78±0.02	0.247	438717748822	see MT 417
	16.04	31.8	20:33:10.354	+41:13:14.17	7.21±0.13	6.75±0.05	6.30±0.04	0.498	···	
	16.71	343.9	20:33:09.192	+41:13:16.60	···	···	7.40±0.18	0.684	438717769429	see MT 417
MT 429	···	···	20:33:10.508	+41:22:22.46	···	···	···	···	438717759391	
	0.08	26.4	20:33:10.511	+41:22:22.53	1.24±0.15	···	1.11±0.12	0.000	···	FS
	2.30	207.6	20:33:10.413	+41:22:20.42	7.19±0.10	···	7.01±0.17	0.031	···	
	6.54	67.8	20:33:11.046	+41:22:24.93	5.57±0.04	···	3.68±0.03	0.048	438717759395	
	8.98	315.4	20:33:09.948	+41:22:28.85	6.69±0.08	···	5.90±0.09	0.248	438717759392	
	10.89	222.0	20:33:09.860	+41:22:14.37	6.66±0.07	···	5.25±0.07	0.280	438717759078	
	10.91	290.2	20:33:09.599	+41:22:26.23	7.05±0.09	···	6.01±0.10	0.355	438717759307	
	12.99	6.2	20:33:10.633	+41:22:35.37	5.51±0.04	···	5.24±0.06	0.372	438717759506	
	13.15	29.3	20:33:11.080	+41:22:33.93	···	···	5.45±0.12	0.403	···	
MT 431	···	···	20:33:10.749	+41:15:08.19	···	···	···	···	438717751166	CygOB2- 9
	5.29	250.5	20:33:10.307	+41:15:06.42	···	···	6.90±0.26	0.029	···	
MT 448	···	···	20:33:13.265	+41:13:28.74	···	···	···	···	438717749007	
	3.69	312.3	20:33:13.023	+41:13:31.23	···	···	8.07±0.16	0.084	···	
	5.44	288.3	20:33:12.807	+41:13:30.46	···	···	7.59±0.13	0.140	438717749013	
	5.91	163.8	20:33:13.411	+41:13:23.07	···	···	9.02±0.31	0.300	···	
	6.05	166.9	20:33:13.386	+41:13:22.85	···	···	8.31±0.19	0.233	438717749012	
	8.17	179.7	20:33:13.268	+41:13:20.57	···	···	8.60±0.23	0.427	···	
	9.34	181.0	20:33:13.251	+41:13:19.40	8.15±0.17	···	7.17±0.11	0.304	438717749011	
	9.36	275.6	20:33:12.439	+41:13:29.66	8.21±0.19	···	8.28±0.19	0.465	438717749008	
	10.26	146.4	20:33:13.767	+41:13:20.20	7.64±0.14	···	7.78±0.14	0.445	438717748625	
	10.41	247.3	20:33:12.413	+41:13:24.73	···	···	7.85±0.15	0.466	···	
	10.42	355.2	20:33:13.188	+41:13:39.13	6.83±0.07	···	5.80±0.06	0.227	438717749009	
	10.46	250.9	20:33:12.388	+41:13:25.31	···	···	8.66±0.24	0.609	···	
	10.62	125.7	20:33:14.029	+41:13:22.55	···	···	8.65±0.24	0.618	438717748653	
	10.77	11.3	20:33:13.451	+41:13:39.30	···	···	8.46±0.21	0.595	438717764537	
	11.68	56.4	20:33:14.127	+41:13:35.20	···	···	8.15±0.18	0.599	438717748926	
	11.72	217.7	20:33:12.629	+41:13:19.48	···	···	6.93±0.10	0.400	438717748619	
	13.14	125.6	20:33:14.211	+41:13:21.09	7.20±0.09	···	6.81±0.10	0.459	438717748659	
MT 455	···	···	20:33:13.690	+41:13:05.78	···	···	···	···	438717748496	
	3.16	208.3	20:33:13.557	+41:13:03.00	···	···	7.04±0.12	0.043	···	

Table 4 *continued on next page*

Table 4 *(continued)*

Field Name	ρ (arcsec)	θ (deg)	R.A. (HH:MM:SS)	Dec. (DD:MM:SS)	ΔJ (mag)	ΔH (mag)	ΔK (mag)	P_{ca}	UKIDSS Number	Notes
	3.76	43.7	20:33:13.920	+41:13:08.50	7.91±0.19	···	6.74±0.10	0.053	···	
	3.77	72.0	20:33:14.008	+41:13:06.94	···	···	7.60±0.15	0.080	···	
	3.83	63.6	20:33:13.995	+41:13:07.48	···	···	6.99±0.11	0.062	438717764374	
	3.91	65.6	20:33:14.006	+41:13:07.40	···	···	8.15±0.20	0.110	···	
	4.91	1.1	20:33:13.699	+41:13:10.70	8.69±0.33	···	7.42±0.14	0.121	438717764373	
	5.52	173.9	20:33:13.743	+41:13:00.30	7.92±0.20	···	6.29±0.08	0.094	438717748503	
	5.82	106.8	20:33:14.184	+41:13:04.10	6.35±0.08	···	4.97±0.04	0.058	438717748501	
	6.12	137.5	20:33:14.057	+41:13:01.27	···	···	7.26±0.13	0.169	438717764371	
	6.23	270.3	20:33:13.138	+41:13:05.82	5.14±0.04	···	4.80±0.04	0.061	···	
	6.51	270.9	20:33:13.114	+41:13:05.88	3.39±0.02	···	2.96±0.02	0.019	438717748504	
	6.71	162.1	20:33:13.873	+41:12:59.40	7.04±0.11	···	5.89±0.06	0.118	438717748502	
	9.03	282.5	20:33:12.909	+41:13:07.73	···	···	6.37±0.08	0.238	438717748500	
	9.37	310.6	20:33:13.060	+41:13:11.88	6.53±0.08	···	5.55±0.06	0.190	438717748497	
	11.43	117.7	20:33:14.587	+41:13:00.47	···	···	7.04±0.12	0.441	438717748239	
	12.47	227.5	20:33:12.876	+41:12:57.35	···	···	6.99±0.12	0.491	438717748214	
	13.71	114.0	20:33:14.801	+41:13:00.20	···	···	7.60±0.16	0.667	438717748236	
	14.58	296.2	20:33:12.532	+41:13:12.23	···	···	7.08±0.12	0.619	438717748467	
MT 457	···	···	20:33:14.113	+41:20:21.82	···	···	···	···	438717757158	CygOB2-7
	14.74	359.5	20:33:14.103	+41:20:36.56	···	7.95±0.31	···	···	···	
MT 462	···	···	20:33:14.762	+41:18:41.63	···	···	···	···	438717755442	CygOB2-8B
	0.62	229.9	20:33:14.720	+41:18:41.23	···	···	5.44±0.05	0.000	···	
	2.78	306.8	20:33:14.565	+41:18:43.30	···	···	8.34±0.20	0.028	···	
	3.55	9.0	20:33:14.811	+41:18:45.14	···	···	8.22±0.18	0.043	···	
	4.18	298.3	20:33:14.436	+41:18:43.62	···	···	7.40±0.33	0.044	···	
	4.84	202.6	20:33:14.597	+41:18:37.17	6.87±0.10	···	5.93±0.06	0.025	438717755480	
	6.86	81.4	20:33:15.364	+41:18:42.65	···	···	8.67±0.25	0.182	438717766749	
	8.01	34.6	20:33:15.166	+41:18:48.23	5.18±0.04	···	7.63±0.14	0.166	···	
	9.45	22.5	20:33:15.082	+41:18:50.37	-1.09±0.01	···	-1.07±0.01	0.000	438717755482	MT 465
	10.59	21.8	20:33:15.112	+41:18:51.46	3.83±0.02	···	2.36±0.01	0.005	···	see MT 465
	11.28	16.0	20:33:15.038	+41:18:52.47	···	···	8.79±0.28	0.439	···	
	11.91	12.2	20:33:14.986	+41:18:53.27	4.54±0.02	···	4.94±0.04	0.073	438717755484	see MT 465
MT 465	···	···	20:33:15.085	+41:18:50.45	···	···	···	···	438717755482	CygOB2-8A
	1.13	17.3	20:33:15.115	+41:18:51.53	4.87±0.03	4.03±0.03	3.28±0.02	0.000	···	see MT 462
	3.10	339.8	20:33:14.990	+41:18:53.36	5.67±0.05	5.53±0.07	5.55±0.07	0.004	438717755484	see MT 462

Table 4 *continued on next page*

Table 4 *(continued)*

Field Name	ρ (arcsec)	θ (deg)	R.A. (HH:MM:SS)	Dec. (DD:MM:SS)	ΔJ (mag)	ΔH (mag)	ΔK (mag)	P_{ca}	UKIDSS Number	Notes
	7.60	353.6	20:33:15.010	+41:18:58.00	···	···	7.75±0.29	0.098	438717755481	see MT 473
	9.11	311.3	20:33:14.477	+41:18:56.46	6.47±0.11	6.86±0.15	6.54±0.14	0.062	438717755479	
	9.47	202.6	20:33:14.761	+41:18:41.71	1.09±0.01	1.04±0.01	1.09±0.01	0.001	438717755442	MT 462
MT 470	···	···	20:33:15.712	+41:20:17.20	···	···	···	···	438717757137	CygOB2-23
	2.96	275.2	20:33:15.451	+41:20:17.47	3.76±0.02	···	3.76±0.02	0.009	438717757153	
	4.93	356.1	20:33:15.682	+41:20:22.12	7.18±0.11	···	5.92±0.07	0.078	438717757152	
	6.21	19.0	20:33:15.892	+41:20:23.07	···	···	7.64±0.19	0.248	438717767209	
	6.24	236.5	20:33:15.250	+41:20:13.76	8.18±0.22	···	6.17±0.08	0.133	438717757146	
	6.37	102.7	20:33:16.264	+41:20:15.80	5.69±0.05	···	4.87±0.04	0.083	438717757150	
	8.67	13.8	20:33:15.896	+41:20:25.62	3.46±0.01	···	3.34±0.02	0.057	438717757148	
	9.25	64.4	20:33:16.453	+41:20:21.20	7.31±0.12	···	6.98±0.14	0.368	438717757140	
	11.08	244.6	20:33:14.823	+41:20:12.46	7.55±0.17	···	6.97±0.14	0.481	···	
	11.76	225.2	20:33:14.972	+41:20:08.91	···	···	7.03±0.14	0.533	438717756530	
	11.89	249.5	20:33:14.724	+41:20:13.04	6.55±0.07	···	6.11±0.08	0.397	438717757145	
	15.94	177.4	20:33:15.777	+41:20:01.28	6.62±0.08	···	···	···	···	
MT 473	···	···	20:33:16.340	+41:19:01.79	···	···	···	···	438717755476	CygOB2-8D
	2.71	174.1	20:33:16.365	+41:18:59.10	7.25±0.13	···	6.01±0.06	0.021	···	
	3.02	316.9	20:33:16.157	+41:19:04.00	5.58±0.05	···	4.82±0.04	0.015	438717755483	
	4.80	313.8	20:33:16.033	+41:19:05.11	···	···	7.43±0.12	0.114	···	
	5.23	342.0	20:33:16.197	+41:19:06.77	6.99±0.09	···	6.20±0.07	0.081	438717755478	
	5.99	303.0	20:33:15.894	+41:19:05.06	···	···	6.68±0.17	0.124	···	
	7.85	271.3	20:33:15.644	+41:19:01.98	···	···	7.76±0.15	0.317	438717755473	
	8.21	50.2	20:33:16.900	+41:19:07.05	···	···	8.20±0.19	0.404	···	
	8.66	147.0	20:33:16.759	+41:18:54.53	···	···	6.79±0.09	0.251	438717755447	
	8.97	47.6	20:33:16.928	+41:19:07.84	···	···	7.67±0.14	0.379	438717755302	
	10.39	77.9	20:33:17.242	+41:19:03.98	···	···	8.23±0.20	0.568	···	
	10.58	83.3	20:33:17.273	+41:19:03.02	···	···	8.48±0.23	0.626	438717770162	
	11.06	136.4	20:33:17.017	+41:18:53.79	···	···	8.47±0.23	0.657	438717755007	
	12.83	66.7	20:33:17.386	+41:19:06.87	···	···	7.02±0.11	0.509	438717755292	
	13.53	325.8	20:33:15.665	+41:19:12.98	···	···	8.01±0.18	0.722	438717755464	
	15.50	255.9	20:33:15.006	+41:18:58.02	6.49±0.07	···	···	···	438717755481	see MT 465
MT 480	···	···	20:33:17.482	+41:17:09.31	···	···	···	···	438717753113	CygOB2-24
	3.72	201.4	20:33:17.362	+41:17:05.85	···	···	8.70±0.25	0.097	···	
	4.22	320.0	20:33:17.242	+41:17:12.54	···	···	6.84±0.09	0.054	438717766019	

Table 4 *continued on next page*

Table 4 *(continued)*

Field Name	ρ (arcsec)	θ (deg)	R.A. (HH:MM:SS)	Dec. (DD:MM:SS)	ΔJ (mag)	ΔH (mag)	ΔK (mag)	P_{ca}	UKIDSS Number	Notes
	5.70	52.2	20:33:17.882	+41:17:12.80	···	···	8.57±0.24	0.201	···	
	6.00	46.1	20:33:17.866	+41:17:13.47	···	···	8.34±0.20	0.199	···	
	6.50	1.8	20:33:17.500	+41:17:15.80	···	···	8.28±0.20	0.223	438717753118	
	8.81	150.7	20:33:17.865	+41:17:01.63	···	···	6.11±0.07	0.164	438717753111	
	9.32	52.3	20:33:18.136	+41:17:15.01	···	···	6.75±0.09	0.232	438717753115	
	10.46	204.2	20:33:17.102	+41:16:59.76	···	···	5.95±0.06	0.208	438717752802	
	11.48	242.0	20:33:16.583	+41:17:03.91	···	···	4.22±0.03	0.086	438717753112	
	15.10	230.3	20:33:16.452	+41:16:59.66	···	···	5.92±0.06	0.380	···	
MT 483	···	···	20:33:17.988	+41:18:31.10	···	···	···	···	438717755459	CygOB2-8C
	1.71	35.9	20:33:18.077	+41:18:32.49	···	···	8.24±0.22	0.010	···	
	10.40	184.9	20:33:17.909	+41:18:20.74	5.31±0.05	5.18±0.05	5.17±0.05	0.066	438717755477	
	10.47	248.6	20:33:17.123	+41:18:27.28	6.28±0.07	5.09±0.05	5.01±0.05	0.060	438717755461	
MT 485	···	···	20:33:18.032	+41:21:36.65	···	···	···	···	438717770410	
	5.39	281.9	20:33:17.563	+41:21:37.76	···	···	7.44±0.12	0.135	438717758442	
	6.07	342.1	20:33:17.866	+41:21:42.43	···	···	7.28±0.11	0.156	438717758441	
	6.44	314.4	20:33:17.623	+41:21:41.16	···	···	6.56±0.08	0.130	438717758440	
	8.43	275.5	20:33:17.287	+41:21:37.45	···	···	6.06±0.06	0.180	438717758439	
	8.80	277.8	20:33:17.258	+41:21:37.84	···	···	8.22±0.19	0.431	···	
	9.57	124.8	20:33:18.729	+41:21:31.18	···	···	6.75±0.09	0.282	···	
	9.70	124.6	20:33:18.741	+41:21:31.14	···	···	6.27±0.07	0.247	438717758436	
	11.68	98.1	20:33:19.059	+41:21:35.01	···	···	5.04±0.04	0.206	438717758437	
	13.02	241.6	20:33:17.014	+41:21:30.46	···	···	4.41±0.04	0.170	438717758178	
MT 507	···	···	20:33:21.020	+41:17:40.14	···	···	···	···	438717753684	
	2.86	132.7	20:33:21.206	+41:17:38.20	···	···	6.71±0.11	0.037	···	
	3.12	80.0	20:33:21.292	+41:17:40.68	···	···	7.81±0.20	0.073	···	
	7.69	274.4	20:33:20.339	+41:17:40.73	···	···	8.19±0.28	0.427	···	
	8.63	161.3	20:33:21.265	+41:17:31.96	···	···	6.33±0.09	0.247	438717753683	
	8.70	268.1	20:33:20.248	+41:17:39.85	···	···	7.32±0.16	0.373	438717753685	
	9.54	22.2	20:33:21.340	+41:17:48.97	···	···	5.43±0.06	0.219	438717753738	
MT 516	···	···	20:33:23.460	+41:09:13.02	···	···	···	···	438261603293	
	0.73	324.7	20:33:23.423	+41:09:13.62	0.09±0.01	0.04±0.01	-0.04±0.01	0.000	···	
	4.43	307.7	20:33:23.150	+41:09:15.73	4.67±0.02	3.48±0.02	3.09±0.02	0.001	438261603310	
	12.09	271.0	20:33:22.389	+41:09:13.23	6.03±0.05	5.46±0.05	5.22±0.08	0.064	438261603307	
MT 531	···	···	20:33:25.564	+41:33:27.00	···	···	···	···	438768305327	CygOB2-25

Table 4 *continued on next page*

Table 4 *(continued)*

Field Name	ρ (arcsec)	θ (deg)	R.A. (HH:MM:SS)	Dec. (DD:MM:SS)	ΔJ (mag)	ΔH (mag)	ΔK (mag)	P_{ca}	UKIDSS Number	Notes
	1.41	47.6	20:33:25.657	+41:33:27.95	0.52±0.01	···	0.69±0.01	0.000	438768318937	
	4.14	279.7	20:33:25.201	+41:33:27.69	7.41±0.12	···	5.82±0.06	0.031	438768305334	
	5.21	133.9	20:33:25.898	+41:33:23.39	6.62±0.07	···	6.26±0.07	0.062	438768305333	
	7.04	356.6	20:33:25.526	+41:33:34.03	6.06±0.05	···	5.05±0.04	0.055	438768305332	
	12.36	226.8	20:33:24.762	+41:33:18.54	···	···	6.10±0.07	0.280	438768305329	
MT 534	···	···	20:33:26.749	+41:10:59.51	···	···	···	···	438261604910	
	4.94	283.0	20:33:26.323	+41:11:00.62	···	···	6.53±0.09	0.080	438261604917	
	6.99	152.9	20:33:27.032	+41:10:53.29	···	···	8.20±0.23	0.303	438261604913	
	7.29	99.7	20:33:27.386	+41:10:58.29	···	···	7.86±0.19	0.283	438261604916	
	12.78	42.7	20:33:27.518	+41:11:08.90	···	···	7.40±0.15	0.559	···	
	13.38	43.5	20:33:27.566	+41:11:09.21	···	···	4.27±0.04	0.168	438261604912	
MT 555	···	···	20:33:30.307	+41:35:57.89	···	···	···	···	438768323683	CygOB2-74
	3.94	252.7	20:33:29.971	+41:35:56.72	···	···	8.38±0.22	0.090	···	
	6.82	279.0	20:33:29.706	+41:35:58.96	···	···	5.84±0.06	0.086	438768323687	
	7.22	193.2	20:33:30.160	+41:35:50.87	···	···	5.84±0.06	0.096	438768323686	
MT 556	···	···	20:33:30.785	+41:15:22.66	···	···	···	···	438717751402	CygOB2-18
	0.66	73.4	20:33:30.841	+41:15:22.85	···	···	4.86±0.05	0.000	···	
	6.66	246.7	20:33:30.243	+41:15:20.02	···	···	8.54±0.38	0.113	438717751411	
	9.56	43.3	20:33:31.367	+41:15:29.61	8.20±0.23	···	7.33±0.16	0.122	438717751410	
	10.20	38.0	20:33:31.343	+41:15:30.69	···	···	9.09±0.63	0.292	···	
	10.36	200.6	20:33:30.462	+41:15:12.96	7.41±0.15	···	7.26±0.16	0.135	438717751408	
MT 588	···	···	20:33:37.001	+41:16:11.30	···	···	···	···	438717752046	
	2.25	112.0	20:33:37.186	+41:16:10.46	···	···	6.68±0.09	0.017	···	
	3.43	121.5	20:33:37.261	+41:16:09.51	···	···	7.01±0.10	0.043	···	
	3.46	323.1	20:33:36.817	+41:16:14.06	···	···	7.47±0.13	0.054	···	
	4.54	259.7	20:33:36.605	+41:16:10.49	···	···	8.41±0.22	0.140	···	
	5.43	197.1	20:33:36.859	+41:16:06.11	···	···	8.31±0.26	0.186	438717769885	
	7.22	350.0	20:33:36.890	+41:16:18.41	···	···	8.07±0.18	0.276	438717765634	
	8.03	93.8	20:33:37.712	+41:16:10.77	···	···	7.49±0.13	0.260	438717752048	
	8.05	146.0	20:33:37.400	+41:16:04.63	···	···	7.34±0.12	0.245	438717752045	
	9.28	215.1	20:33:36.528	+41:16:03.71	···	···	7.40±0.13	0.319	438717752044	
	12.57	74.9	20:33:38.078	+41:16:14.58	···	···	8.74±0.30	0.742	···	
MT 601	···	···	20:33:39.109	+41:19:25.86	···	···	···	···	438717766878	CygOB2-19
	1.87	245.5	20:33:38.958	+41:19:25.08	3.89±0.02	···	4.27±0.03	0.001	438717756038	

Table 4 *continued on next page*

Table 4 *(continued)*

Field Name	ρ (arcsec)	θ (deg)	R.A. (HH:MM:SS)	Dec. (DD:MM:SS)	ΔJ (mag)	ΔH (mag)	ΔK (mag)	P_{ca}	UKIDSS Number	Notes
	3.37	354.6	20:33:39.081	+41:19:29.21	···	···	8.92±0.35	0.051	···	
	6.55	111.3	20:33:39.651	+41:19:23.47	5.66±0.05	···	6.13±0.07	0.049	···	
	6.60	110.5	20:33:39.658	+41:19:23.54	5.74±0.06	···	5.73±0.06	0.037	438717756053	
	6.92	1.6	20:33:39.126	+41:19:32.78	···	···	6.86±0.23	0.085	···	
	7.59	292.9	20:33:38.489	+41:19:28.81	6.29±0.07	···	6.29±0.08	0.073	438717756051	MT 599
	7.70	356.8	20:33:39.071	+41:19:33.54	7.20±0.14	···	6.02±0.07	0.062	438717756054	
	7.93	98.5	20:33:39.806	+41:19:24.68	···	···	8.35±0.25	0.201	438717756052	
	11.44	306.6	20:33:38.294	+41:19:32.67	···	···	8.03±0.21	0.340	438717756044	
	13.50	206.7	20:33:38.571	+41:19:13.80	···	···	7.46±0.15	0.370	438717755405	
	14.25	172.3	20:33:39.280	+41:19:11.74	5.06±0.04	···	···	···	438717785957	
MT 605	···	···	20:33:39.799	+41:22:52.38	···	···	···	···	438717760019	
	0.10	258.0	20:33:39.790	+41:22:52.36	0.64±0.04	···	0.73±0.05	0.000	···	FS
	3.91	334.1	20:33:39.647	+41:22:55.90	···	···	8.21±0.26	0.113	···	
	7.22	320.7	20:33:39.392	+41:22:57.97	···	···	6.02±0.12	0.142	438717798666	
	7.49	305.3	20:33:39.256	+41:22:56.72	···	···	7.42±0.17	0.259	438717760020	
	7.72	149.7	20:33:40.144	+41:22:45.72	···	···	7.69±0.19	0.305	438717760018	
	8.61	305.6	20:33:39.177	+41:22:57.39	···	···	7.13±0.14	0.291	438717760015	
	9.14	47.2	20:33:40.395	+41:22:58.59	···	···	7.28±0.15	0.341	438717760008	
	9.82	47.0	20:33:40.437	+41:22:59.08	···	···	8.26±0.28	0.540	438717786639	
MT 611	···	···	20:33:40.868	+41:30:18.98	···	···	···	···	438768328390	
	1.91	136.8	20:33:40.985	+41:30:17.59	5.84±0.06	···	4.80±0.04	0.007	···	
	3.78	290.9	20:33:40.554	+41:30:20.33	6.76±0.10	···	4.71±0.04	0.026	438768328393	
	6.19	170.2	20:33:40.962	+41:30:12.88	···	···	8.10±0.23	0.285	438768335588	
	7.72	36.4	20:33:41.276	+41:30:25.19	···	···	7.20±0.14	0.286	438768328391	
	8.11	63.4	20:33:41.514	+41:30:22.61	···	···	7.61±0.30	0.365	438768328389	
	9.20	202.1	20:33:40.560	+41:30:10.46	···	···	7.78±0.19	0.470	438768328409	
	11.04	35.7	20:33:41.441	+41:30:27.95	6.58±0.09	···	6.27±0.09	0.359	438768328388	
	12.16	328.5	20:33:40.303	+41:30:29.35	7.44±0.16	···	6.84±0.12	0.505	438768328172	
MT 632	···	···	20:33:46.103	+41:33:01.05	···	···	···	···	438768326471	CygOB2-10
	0.21	246.2	20:33:46.085	+41:33:00.97	2.40±0.58	···	2.80±0.78	0.000	···	FS
	0.74	179.2	20:33:46.103	+41:33:00.31	···	···	5.24±0.05	0.000	···	
	4.16	351.3	20:33:46.046	+41:33:05.17	5.94±0.05	···	6.03±0.07	0.010	438768326479	
MT 642	···	···	20:33:47.835	+41:20:41.54	···	···	···	···	438717788537	CygOB2-26
	0.32	41.9	20:33:47.854	+41:20:41.78	4.27±1.82	···	5.22±2.73	0.000	···	FS

Table 4 *continued on next page*

Table 4 *(continued)*

Field Name	ρ (arcsec)	θ (deg)	R.A. (HH:MM:SS)	Dec. (DD:MM:SS)	ΔJ (mag)	ΔH (mag)	ΔK (mag)	P_{ca}	UKIDSS Number	Notes
	1.73	190.3	20:33:47.808	+41:20:39.84	···	···	7.80±0.15	0.011	···	
	5.79	199.9	20:33:47.660	+41:20:36.10	6.94±0.11	···	6.81±0.10	0.085	438717788548	
	14.57	49.1	20:33:48.813	+41:20:51.08	···	···	7.74±0.17	0.548	438717788539	
MT 692	···	···	20:33:59.251	+41:05:38.09	···	···	···	···	438261839361	
	2.61	54.6	20:33:59.439	+41:05:39.60	···	···	5.29±0.05	0.022	438261853756	
	3.16	224.1	20:33:59.057	+41:05:35.82	···	···	4.83±0.04	0.027	438261853755	
	6.36	88.1	20:33:59.813	+41:05:38.31	···	···	5.53±0.05	0.135	438261839360	
	9.39	29.4	20:33:59.659	+41:05:46.26	···	···	6.64±0.10	0.412	438261839312	
	9.51	109.6	20:34:00.044	+41:05:34.90	···	···	7.54±0.16	0.570	438261839377	
	10.53	234.9	20:33:58.489	+41:05:32.03	···	···	7.75±0.18	0.682	438261839117	
	10.65	307.5	20:33:58.503	+41:05:44.57	···	···	8.09±0.23	0.749	···	
	11.69	284.9	20:33:58.252	+41:05:41.09	···	···	6.36±0.08	0.512	···	
	11.83	297.5	20:33:58.323	+41:05:43.54	···	···	1.47±0.01	0.050	438261839359	
MT 696	···	···	20:33:59.528	+41:17:35.48	···	···	···	···	438717790687	CygOB2-27
	0.82	47.5	20:33:59.582	+41:17:36.04	···	···	4.76±0.03	0.001	···	
	7.06	315.4	20:33:59.088	+41:17:40.51	···	···	8.87±0.31	0.360	438717800777	
	7.39	285.4	20:33:58.895	+41:17:37.45	···	···	5.46±0.05	0.097	438717790696	
	8.92	310.8	20:33:58.929	+41:17:41.31	···	···	7.88±0.17	0.356	438717790694	
	9.43	235.3	20:33:58.840	+41:17:30.12	···	···	7.90±0.24	0.392	438717790695	
	10.58	228.5	20:33:58.825	+41:17:28.47	···	···	8.44±0.24	0.557	438717790692	
	11.12	32.7	20:34:00.060	+41:17:44.84	···	···	6.05±0.07	0.269	438717790693	
MT 716	···	···	20:34:04.861	+41:05:12.92	···	···	···	···	438261840310	CygOB2-41
	1.53	243.1	20:34:04.740	+41:05:12.23	···	···	5.65±0.06	0.007	···	
	1.88	76.6	20:34:05.023	+41:05:13.36	···	···	6.49±0.12	0.016	···	
	3.46	218.0	20:34:04.672	+41:05:10.19	···	···	7.28±0.11	0.075	···	
	5.03	239.2	20:34:04.479	+41:05:10.35	···	···	5.49±0.05	0.072	438261840314	
	5.26	240.5	20:34:04.456	+41:05:10.33	···	···	6.68±0.08	0.127	···	
	5.71	36.3	20:34:05.160	+41:05:17.52	···	···	9.37±0.36	0.446	···	
	6.78	258.1	20:34:04.275	+41:05:11.52	···	···	7.17±0.10	0.248	438261840312	
	7.10	45.3	20:34:05.308	+41:05:17.91	···	···	5.85±0.05	0.157	438261840313	
	8.07	179.5	20:34:04.867	+41:05:04.85	···	···	6.73±0.08	0.279	···	
	8.13	191.1	20:34:04.723	+41:05:04.94	···	···	1.49±0.01	0.023	438261840315	MT 715
	11.59	123.7	20:34:05.714	+41:05:06.50	···	···	8.10±0.16	0.731	438261840331	
	12.53	159.7	20:34:05.246	+41:05:01.17	···	···	7.30±0.11	0.646	438261840311	

Table 4 *continued on next page*

Table 4 *(continued)*

Field Name	ρ (arcsec)	θ (deg)	R.A. (HH:MM:SS)	Dec. (DD:MM:SS)	ΔJ (mag)	ΔH (mag)	ΔK (mag)	P_{ca}	UKIDSS Number	Notes
	12.68	327.8	20:34:04.264	+41:05:23.66	···	···	7.51±0.12	0.692	438261840079	
	13.14	86.0	20:34:06.020	+41:05:13.83	···	···	6.46±0.07	0.532	438261840405	
	14.93	264.6	20:34:03.546	+41:05:11.51	···	···	7.45±0.12	0.796	438261839983	
	15.03	268.6	20:34:03.532	+41:05:12.55	···	···	7.66±0.13	0.832	···	
MT 734	···	···	20:34:08.501	+41:36:59.24	···	···	···	···	438768332783	CygOB2-11
	11.28	241.9	20:34:07.615	+41:36:53.92	···	···	7.90±0.23	0.270	···	
MT 736	···	···	20:34:09.519	+41:34:13.69	···	···	···	···	438768325130	CygOB2-75
	5.99	51.3	20:34:09.936	+41:34:17.43	3.80±0.02	···	3.38±0.02	0.027	438768325131	
	13.06	126.6	20:34:10.454	+41:34:05.91	···	···	7.38±0.25	0.657	438768325128	
MT 745	···	···	20:34:13.510	+41:35:02.73	···	···	···	···	438768324434	CygOB2-29
	2.81	260.5	20:34:13.262	+41:35:02.26	···	···	6.22±0.07	0.022	···	
	11.41	85.1	20:34:14.523	+41:35:03.69	···	···	6.65±0.09	0.344	438768324433	
MT 771	···	···	20:34:29.596	+41:31:45.54	···	···	···	···	438768327363	
	2.31	180.4	20:34:29.595	+41:31:43.23	4.92±0.03	···	4.87±0.04	0.003	438768338357	
	5.18	109.4	20:34:30.031	+41:31:43.82	7.03±0.15	···	7.23±0.12	0.066	438768327371	
	6.83	210.4	20:34:29.288	+41:31:39.65	···	···	8.25±0.22	0.160	438768327370	
	9.51	275.3	20:34:28.753	+41:31:46.41	···	···	8.37±0.25	0.301	438768327369	
MT 793	···	···	20:34:43.581	+41:29:04.63	···	···	···	···	438717664510	CygOB2-30
	4.82	28.9	20:34:43.788	+41:29:08.85	···	···	7.91±0.20	0.112	438717673057	
	6.38	297.4	20:34:43.077	+41:29:07.57	8.08±0.22	···	7.54±0.16	0.160	438717664513	
	6.61	197.8	20:34:43.401	+41:28:58.34	4.23±0.02	···	4.19±0.03	0.030	438717664514	
	9.08	303.2	20:34:42.905	+41:29:09.60	···	···	6.64±0.10	0.217	438717664509	
	9.61	318.3	20:34:43.012	+41:29:11.81	···	···	7.76±0.19	0.356	438717670531	
	9.90	238.1	20:34:42.833	+41:28:59.40	6.92±0.10	···	4.40±0.03	0.076	438717664511	
S 3	···	···	20:31:37.499	+41:13:21.03	···	···	···	···	438717693112	
	3.97	214.3	20:31:37.300	+41:13:17.75	2.66±0.01	2.81±0.01	3.01±0.02	0.001	438717693097	
	8.19	166.4	20:31:37.670	+41:13:13.07	···	7.50±0.13	6.91±0.14	0.078	438717693111	
	11.75	268.7	20:31:36.458	+41:13:20.75	6.51±0.07	···	6.67±0.12	0.131	438717693108	
S 5	···	···	20:32:22.425	+41:18:19.09	···	···	···	···	438717697625	CygOB2-5A
	0.93	55.2	20:32:22.493	+41:18:19.62	···	···	3.09±0.02	0.000	···	CygOB2-5B
	5.55	225.7	20:32:22.073	+41:18:15.22	···	···	4.68±0.04	0.001	438717697644	CygOB2-5D
S 73	···	···	20:34:21.930	+41:17:01.60	···	···	···	···	438717794248	
	0.56	117.7	20:34:21.975	+41:17:01.34	···	···	4.63±2.14	0.000	···	FS
	2.87	65.1	20:34:22.161	+41:17:02.81	···	···	8.23±0.23	0.046	···	

Table 4 *continued on next page*

Table 4 *(continued)*

Field Name	ρ (arcsec)	θ (deg)	R.A. (HH:MM:SS)	Dec. (DD:MM:SS)	ΔJ (mag)	ΔH (mag)	ΔK (mag)	P_{ca}	UKIDSS Number	Notes
	3.26	106.9	20:34:22.207	+41:17:00.66	···	···	7.23±0.13	0.037	438717806985	
	4.44	20.8	20:34:22.070	+41:17:05.75	···	···	8.56±0.29	0.124	438717806983	
	4.70	49.7	20:34:22.248	+41:17:04.64	···	···	7.73±0.19	0.094	438717806984	
	5.50	28.2	20:34:22.161	+41:17:06.45	···	···	8.13±0.22	0.152	438717806982	
	6.62	41.9	20:34:22.323	+41:17:06.52	···	···	7.08±0.12	0.138	438717794262	
	8.45	185.0	20:34:21.865	+41:16:53.19	···	···	4.70±0.04	0.064	438717794263	
	8.45	284.8	20:34:21.206	+41:17:03.77	···	···	7.41±0.15	0.239	438717794258	
	8.99	268.2	20:34:21.133	+41:17:01.32	···	···	6.62±0.10	0.205	438717794261	
	11.52	9.1	20:34:22.092	+41:17:12.98	···	···	6.85±0.11	0.337	438717794250	
	12.50	166.3	20:34:22.193	+41:16:49.46	···	···	6.47±0.09	0.343	438717794254	
WR 145	···	···	20:32:06.285	+40:48:29.55	···	···	···	···	438718045765	
	12.51	80.5	20:32:07.372	+40:48:31.62	···	···	8.35±0.18	0.400	438718045770	

3.1. *Astrometry*

The calibration of the astrometric transformation from pixel position of the PSF peak to the coordinates of the star is described in Appendix A. The celestial coordinates reported in Table 4 are based upon the 2MASS coordinates of the primaries (Skrutskie et al. 2006) and the relative SExtractor positions from the NIRI K-band images. We caution that in a few cases where a bright close companion exists, the 2MASS position refers to the center of light of the flux blend, so the coordinates for all the associated companions target may have small systematic offsets in such cases. However, the relative coordinate offsets from the main target derived from (ρ, θ) are reliable even in these cases. The astrometry information listed for MT 421 includes a few stars that were only observed with the PHARO camera, and for those the position on the Palomar K_S-band frame is used.

The uncertainties in the separation ρ depend primarily on the pixel scale (known within 0.1%), non-linearity in the pixel scale (increasing uncertainty with separation), and uncertainties in centroid fitting where the PSFs of close pairs overlap. In general, the uncertainty in ρ is less than $0\farcs07$. The position angle has a systematic uncertainty of $0\fdg1$ and a measurement uncertainty that is inversely proportional to ρ (generally less than $0\fdg6/\rho('')$ in the absence of pair blending).

3.2. *Photometry*

Most of the companions detected have separations $\rho > 0\farcs5$, and for these we relied upon the aperture photometry from SExtractor. We describe in Appendix B how the differential photometry calibration is accomplished by construction of enclosed energy curves for nine apertures of successively larger diameter for each detected star. We select from these measurements the aperture result with the largest S/N ratio and then apply an appropriate aperture correction. The aperture correction is based upon the radial distance of the star from the center of the FOV and the seeing at the time of the observation, so that a first order correction may be made for the PSF degradation (lower Strehl ratio) with increasing off axis position. Stars detected near the periphery of the FOV were measured in specially constructed edge-images that were formed from a subset of observations with optimized dither positions. Note that in the case of MT 421 the photometry is derived from the PHARO camera alone, because the NIRI results were limited to the K-band.

There are also close systems with separations $\rho < 0\farcs5$, where the companion falls within the halo of the primary's PSF. There are a total of nine such systems in our sample: A 20, A 26, A 41, MT 5, MT 429, MT 605, MT 632, MT 642, and Schulte 73. The PSFs are too blended for these close systems to use the aperture photometry performed by SExtractor. Instead, the photometric measurements were made using the program FITSTARS, a PSF deconvolution program (ten Brummelaar et al. 1996, 2000). FITSTARS fits blended PSFs to estimate the relative magnitudes and positions of the two components. The code begins with a PSF estimate from an image of single star, and then uses an iterative scheme to improve the specific PSF shape based upon the image of the binary star. The outer wings of the PSF are constrained to be spherically symmetric. The positions and amplitudes of the PSF for each component are optimized to minimize the residuals between the observations and model fit. Numerical tests with artificial companions are used to estimate the uncertainties in relative position and intensity. Visual inspection of the residuals indicated that a simple two-component fit was adequate in each of the nine cases where FITSTARS was applied.

4. DETECTION OF PHYSICAL COMPANIONS

4.1. *Detection Limits*

We made one epoch imaging of 74 O- and B-type stars in Cyg OB2 with high angular resolution methods in the infrared JHK bands, and we found at least one star in the field around each of our targets, for a total of 546 possible companions. We present in Table 4 photometric and positional information for stars found in the field around our targets. Figure 1 shows the dynamical range of our detections as a function of separation. This figure demonstrates the sensitivity and completeness of our survey. The separation axis is plotted as $\log \rho$ to show the sensitivity at both close and large distances. The closest pair resolved was the binary MT 429 with $\rho = 0\overset{\prime\prime}{.}08$ (3.6 pixels), while the largest separation was $\rho = 16\overset{\prime\prime}{.}71$ for a distant star in the FOV of MT 421. The relatively faintest companion (of MT 716) has a magnitude difference of $\Delta K = 9.37$ mag. The dotted lines in Figure 1 show the approximate limits for detection in our sample that are bounded by the largest contrast ratio at the bottom, half of the square FOV on the right, and the restriction to brighter companions at closer separation on the left. The limiting dotted line in Figure 1 is substantially the same as the detection limit found by Lafrenière et al. (2014) (see their Fig. 1) who calculated the standard deviation as a function of separation in annuli of residual images with companions removed. The work by Lafrenière et al. (2014) is based upon the same NIRI/ALTAIR camera system as we used, and their target sample spans a similar magnitude range, and thus their detection threshold is essentially the same as we plot in Figure 1. Note that the exposure times were selected to obtain a uniform S/N ratio for all the targets, so the detection limits are generally the same for bright and faint targets (Table 3 documents the relatively small differences in image quality and Strehl ratio between observations). The faint limit shown in Figure 1 applies generally to parts of the co-added image with $\rho < 10''$, and detection limit is degraded in the outer parts where the sky is only recorded in a subset of the dither positions.

We performed several numerical experiments where we created artificial binaries to test the detection limits. The lower limit of magnitude as a function of separation was similar to the area bounded by the dotted lines in Figure 1.

4.2. *Probable Bound Companions*

Ideally we would like to differentiate between chance alignments and gravitationally bound systems. The best way to do so is to obtain multi-epoch observations, in conjunction with a proper motion study and spectroscopic information about the companions. However, for this study we have only a single epoch observation and JHK color information. In Figure 2, we show the number density (number arcsec^{-2}) of companions for the entire sample as a function of separation. The companion density levels off at a separation of $\rho \approx 4''$. This very likely corresponds to the average number density of stars in the association and along this line of sight. Stars found at separations $\rho > 4''$ are more likely to be chance alignments. However, the surface density increases greatly within $\rho < 1''$, and stars found within this separation are more likely to be physically bound companions.

Since we only have access to single-epoch observations, we may apply a statistical argument developed by Correia et al. (2006) to determine likely companions. The statistical probability that a detected companion is part of the background field of stars in this direction was calculated using the expression from Correia et al. (2006),

$$P_{ca}(\Sigma_K, \rho) = 1 - e^{-\pi \Sigma_K \rho^2}. \tag{1}$$

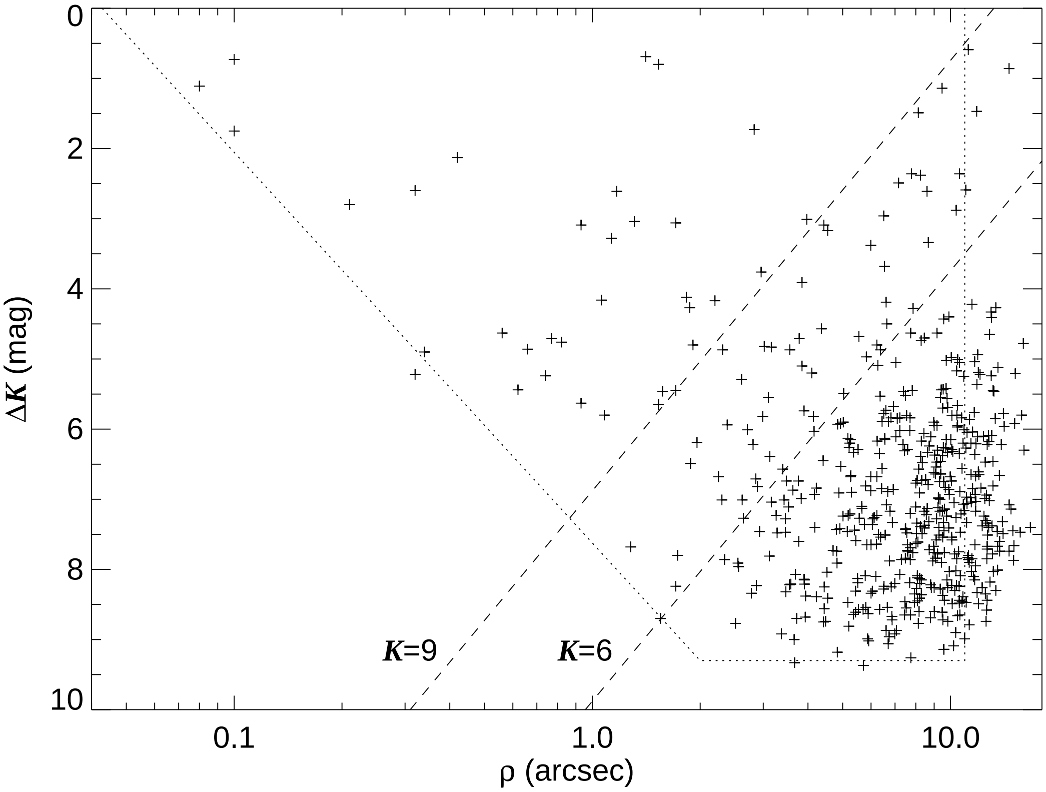

Figure 1. The detected companions as a function of angular separation ρ and magnitude difference ΔK. The dotted lines show the approximate lower limit for positive detection within our sample. The two diagonal dashed lines indicate the lower limits for meeting the chance alignment with background stars criterion $P_{ca} < 1\%$ for primary star magnitude $K = 6$ and 9 mag. Only those companions above both the dotted and dashed lines are included in the assessment of binary statistics.

Here P_{ca} is the probability of finding a field star within a circle with a radius ρ (in arcseconds) centered on the target (subscript "ca" refers to chance alignment). Σ_K is the cumulative surface density of stars (arcsec^{-2}) in the surrounding field that includes all stars brighter than magnitude K. Our working assumption is that if the probability P_{ca} is low, then the detected companion is likely to be physically associated with the target.

The field surface density was determined using a combination of data from 2MASS (Skrutskie et al. 2006) and UKIDSS (Lawrence et al. 2007) of the area surrounding around each of our targets. The 2MASS survey provided photometry for stars with $K < 14$ mag and UKIDSS provided the information for $14 < K < 16$ mag. The magnitudes of faint stars in UKIDSS were set by comparing the magnitudes of stars in the range of $K = 8 - 14$ mag where the 2MASS and UKIDSS sets of observations overlapped. This was done by identifying stars in the UKIDSS frame that had 2MASS K magnitudes. Then the magnitudes of fainter stars were determined from the stars in common with 2MASS and the differential magnitudes measured in the UKIDSS catalog. We formed areal density estimates Σ_K in bins of one magnitude increments for tabular interpolation purposes. The field star counts increase rapidly towards fainter magnitudes, and an approximate linear fit of the mean

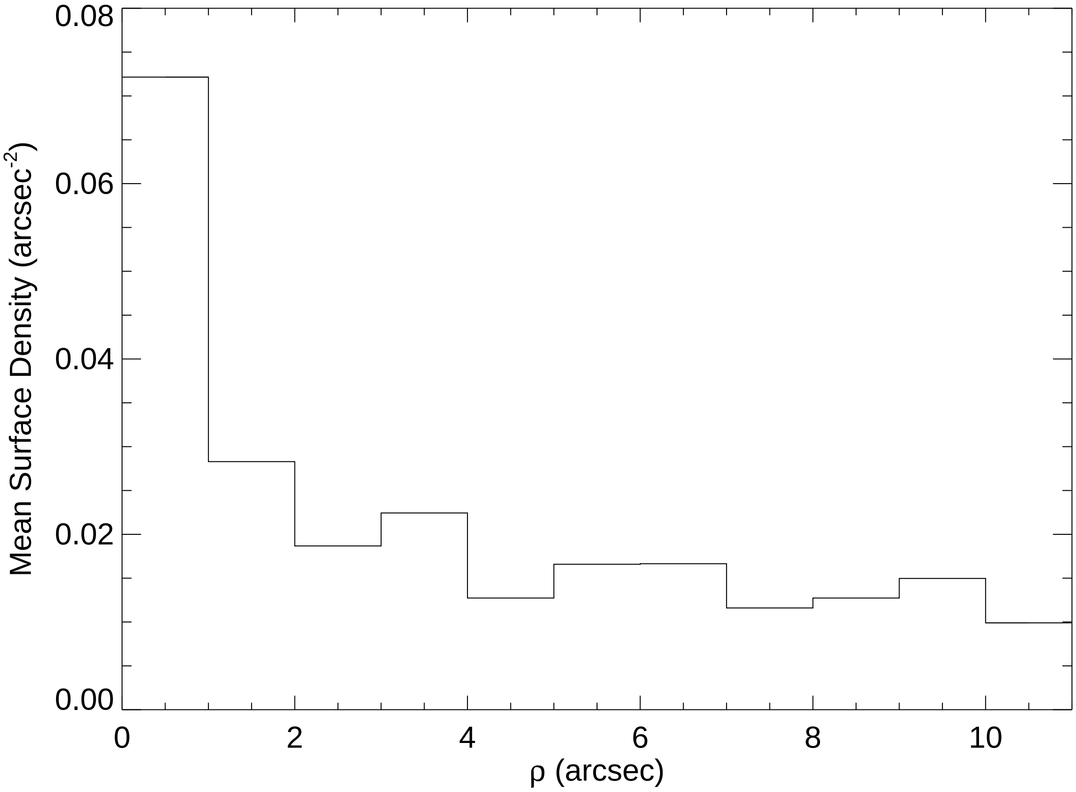

Figure 2. The surface density of stellar companions as a function of angular separation ρ. The peak at small ρ probably corresponds to physical companions, while the numbers at larger distance reflect more the typical star count background in the direction of Cyg OB2. At a distance of 1.33 kpc, $1''$ corresponds to a projected separation of 1330 AU.

star count trend is $\log \Sigma_K = -7.67 + 0.326K$. The binned version of $\log \Sigma_K$ is in good agreement with predicted star counts for the direction of Cyg OB2 from the Besançon model of the Galaxy[2] (Czekaj et al. 2014) over the range of $K = 7$ to 15 mag.

The derived cumulative star count function Σ_K is based on all the stars in the Cyg OB2 fields including the targets and any physical companions. Consequently, Σ_K may overestimate the numbers of field association, foreground, and background stars in the vicinity of the targets, because the physical companions are included. The result is that the probability of finding a field star P_{ca} increases, so that some physical companions may be placed in the field rather than bound categories. Thus, we may be rejecting some physical companions from consideration, especially at the brighter end where the targets and their bound companions contribute most to the net star counts. However, this potential underestimate of the numbers of physical companions is negligible, because the stars in Cyg OB2 are dispersed over a large part of the sky (Wright et al. 2015) and the areal density of bound companions is low. The good match of our empirical Σ_K relation to the Galactic model for background stars confirms that the relative contribution of Cyg OB2 stars to the total star counts

---

[2] https://model.obs-besancon.fr

is low, especially towards fainter stars. Ideally we might consider a star count model that includes components from both the field and bound companions, but the latter would need many apriori assumptions about the number distributions of physical companion mass and separation that are poorly known at present.

We estimated the probability $P_{ca}(\Sigma_K, \rho)$ based upon the companion magnitude K and separation ρ. The K magnitudes of the companions were determined from the 2MASS K_S magnitude of the primary plus the ΔK magnitude from the NIRI observations. Then the predicted field star areal density was estimated by linear interpolation in the $(K, \log \Sigma_K)$ plane (and by extrapolation for the faintest companions). Finally, we used the functional expression for $P_{ca}(\Sigma_K, \rho)$ given above to estimate the field star chance alignment probability for each detected companion. The calculated probability $P_{ca}(\Sigma_K, \rho)$ is listed in column 9 of Table 4. We assume that the companions with $P_{ca}(\Sigma_K, \rho) < 1\%$ are unlikely to be members of the field population, and are instead physical companions located near to their respective target star. The numbers of such probable physical companions are summarized in Table 5 (given in full in the electronic version). The columns give the star name, total number of stars in the NIRI FOV, the number of probable companions, the number of companions found in the *HST*/FGS high angular resolution survey by Caballero-Nieves et al. (2014), the number of close companions found as spectroscopic binaries by Kobulnicky et al. (2014), the total number of all known companions (astrometric and spectroscopic), the number of companions new to this work, and the mass of the central star based upon its position in the H-R diagram from Wright et al. (2015). The companions detected in the *HST*/FGS survey are all confirmed here with the exception of the very close companions of MT 304 ($\rho = 0\farcs064$) and MT 696 ($\rho = 0\farcs023$) that are too close and faint for resolution with NIRI. On the other hand, the NIRI imaging program has revealed fainter companions that eluded detection with FGS. There are 25 new detections in our NIRI survey that were unknown companions prior to this work.

Table 5. Multiplicity Properties

Star (1)	N(FOV) (2)	$N(P_{ca} < 0.01)$ (3)	N(FGS) (4)	N(SB) (5)	N(Total) (6)	N(New) (7)	$M_1/M_\odot$ (8)
A 11	7	3	⋯	1	4	3	34.7
A 12	3	0	⋯	⋯	0	0	⋯
A 15	4	0	⋯	⋯	0	0	31.8
A 18	12	0	⋯	⋯	0	0	⋯
A 20	6	1	⋯	⋯	1	1	35.0
A 23	2	0	0	⋯	0	0	26.3
A 24	3	0	⋯	⋯	0	0	29.6
A 25	7	0	⋯	⋯	0	0	⋯
A 26	7	1	⋯	⋯	1	1	18.7
A 27	3	0	0	⋯	0	0	35.2
A 29	2	0	⋯	⋯	0	0	⋯
A 32	7	0	⋯	⋯	0	0	⋯
A 37	6	0	⋯	⋯	0	0	⋯
A 38	12	1	⋯	⋯	1	1	20.3
A 41	3	1	1	⋯	1	0	⋯
A 46	4	0	0	⋯	0	0	⋯

Table 5 *continued on next page*

Table 5 *(continued)*

Star (1)	N(FOV) (2)	$N(P_{ca} < 0.01)$ (3)	N(FGS) (4)	N(SB) (5)	N(Total) (6)	N(New) (7)	$M_1/M_\odot$ (8)
B 17	5	0	...	1	1	0	24.8
MT 5	16	1	1	0	1	0	...
MT 59	3	1	1	1	2	0	25.5
MT 70	9	0	0	1	1	0	18.4
MT 83	3	0	0	0	0	0	14.3
MT 138	9	1	1	0	1	0	23.6
MT 140	9	0	...	...	...	...	...
MT 145	14	0	0	1	1	0	16.8
MT 213	7	0	0	0	0	0	14.5
MT 217	6	2	0	0	2	1	28.6
MT 227	7	0	0	0	0	0	19.1
MT 250	21	0	0	0	0	0	8.0
MT 258	16	1	0	1	2	1	21.9
MT 259	16	0	0	0	0	0	12.9
MT 299	7	1	0	0	1	1	23.4
MT 304	2	1	1	0	2	0	110.0
MT 317	4	0	0	0	0	0	24.8
MT 339	11	0	0	1	1	0	21.2
MT 376	8	0	0	0	0	0	20.9
MT 390	10	0	0	1	1	0	23.5
MT 403	11	1	0	1	2	1	10.7
MT 417	12	2	2	1	3	0	49.9
MT 421	47	4	...	1	5	1	16.3
MT 429	9	1	1	2	3	0	13.5
MT 431	2	0	0	1	1	0	51.6
MT 448	17	0	0	1	1	0	28.6
MT 455	19	0	0	0	0	0	21.4
MT 457	2	0	0	0	0	0	46.7
MT 462	12	3	0	0	3	1	35.2
MT 465	6	3	0	1	4	0	41.1
MT 470	12	1	0	0	1	1	16.8
MT 473	16	0	0	2	2	0	20.2
MT 480	11	0	0	0	0	0	25.4
MT 483	4	1	0	0	1	1	41.6
MT 485	10	0	0	1	1	0	21.8
MT 507	7	0	0	0	0	0	18.7
MT 516	4	2	1	0	2	1	51.6
MT 531	6	1	1	0	1	0	23.5
MT 534	6	0	0	0	0	0	23.4
MT 555	4	0	0	1	1	0	24.9
MT 556	6	1	0	0	1	1	28.9
MT 588	11	0	0	1	1	0	17.9
MT 601	12	1	0	1	2	1	26.0
MT 605	9	1	1	1	2	0	12.5
MT 611	9	1	0	0	1	1	22.3
MT 632	4	3	1	0	3	2	37.4

Table 5 *continued on next page*

Table 5 *(continued)*

Star (1)	N(FOV) (2)	$N(P_{ca} < 0.01)$ (3)	N(FGS) (4)	N(SB) (5)	N(Total) (6)	N(New) (7)	$M_1/M_\odot$ (8)
MT 642	5	1	0	0	1	1	15.9
MT 692	10	0	0	0	0	0	14.2
MT 696	8	1	1	1	3	1	17.2
MT 716	17	1	···	0	1	1	17.5
MT 734	2	0	0	1	1	0	43.7
MT 736	3	0	0	0	0	0	18.0
MT 745	3	0	0	1	1	0	25.4
MT 771	5	1	0	1	2	1	29.0
MT 793	7	0	0	0	0	0	12.7
S 3	4	1	···	1	2	0	38.0
S 5	3	2	1	2	4	0	93.1
S 73	13	1	0	1	2	1	19.6
WR 145	2	0	0	1	1	0	> 25

Note—
(1) Star Name
(2) Total number of the stars found in the target field.
(3) Number of high probability companion stars from NIRI.
(4) Number of companions detected with FGS.
(5) Number of companions found through radial velocity measurements (Kobulnicky et al. 2014, or for the case of WR 145, Muntean et al. 2009, and references therein).
(6) Total number of unique companions from columns (3) through (5).
(7) New companions detected during this work.
(8) Mass of primary from Wright et al. (2015).

4.3. *Color-Magnitude Diagram of the Companions*

We can determine some facts about the nature of the probable companions by plotting their positions in a near-IR color - magnitude diagram $(J-K, K)$. We constructed such a diagram for those targets with probable companions in the following way. We began by converting the relative magnitudes ΔJ and ΔK to actual magnitudes by adding these to the 2MASS magnitudes J and K_S for the central target. In a few cases we needed to adjust the 2MASS magnitudes to remove the flux of companions within $3''$ of the central star that contributed to the total flux recorded in the lower angular resolution 2MASS measurements. Next we dereddened each of the J and K magnitudes using the reddening associated with the primary target. The reddening values were adopted from one of three sources, listed in Table 1, in order of preference and availability: Negueruela et al. (2008) for $E(J-K)$, Massey & Thompson (1991) for $E(B-V)$, and Torres-Dodgen et al. (1991) for $E(b-y)$. We applied the extinction correction transformations from Fitzpatrick (1999) to convert the adopted reddening to the total extinction in the infrared, A_J and A_K. We adopted the default value of total to selective extinction $R = 3.1$, which is slightly larger than $R = 2.9$ found by Wright et al. (2015). We then combined the two measurements to create the dereddened color index $J-K$. The highest accuracy distance estimates for Cyg OB2 come from interstellar maser parallax measurements by Rygl et al. (2012) and from eclipsing binary dimensions by Kiminki et al. (2015), and we adopted the error weighted mean of their results to arrive at a distance of 1.36 kpc (distance modulus = 10.66 mag). We used this distance to transform the extinction corrected K magnitude to absolute K magnitude. The resulting color - magnitude diagram appears in Figure 3, where the central targets are plotted as gray symbols and the probable companions as black symbols. For the sake of clarity, we omitted several cases with uncertainties in color in excess of 0.9 mag. Also plotted in Figure 3 are theoretical isochrones for three ages from the PARSEC code[3] (Bressan et al. 2012).

We see that most of the central targets are close to the nearly vertical main sequence track, with the exception of the evolved star MT 304 = Cyg OB2 #12 found near the top of the diagram. Likewise, most of the companions also appear as lower mass main sequence stars with implied masses down to $2M_\odot$. There are a few interesting outliers that deserve comment. The companions of MT 258 and MT 299 appear in the very blue and faint part of the color - magnitude diagram, and we suspect that these are less reddened foreground objects rather than physical companions. There are also five very red companion stars that appear to be far from the main sequence. These may be cool field stars, companions that are more reddened than their primary stars, or pre-main sequence stars. Given the youth of Cyg OB2 (1 − 7 Myr; Wright et al. 2015), some of these companions may have retained natal disks that would contribute to their long-wavelength flux.

5. MULTIPLICITY

We can use the total number of probable physical companions (column 3 of Table 5) to determine the multiplicity properites of our sample of 74 massive stars in Cyg OB2. There are 26 single (35%), 27 binary (36%), 12 triple (16%), and 9 higher multiplicity systems (12%). Note that we have essentially double counted the numbers in two cases where companions occur in two adjacent and overlapping fields, MT 213 + MT 217 (Schulte 4A,B) and MT 462 + MT 465 (Schulte 8A,B). The target with the largest number of companions (4) is MT 421 (Schulte 50) that resides at the center

---

[3] http://stev.oapd.inaf.it/cgi-bin/cmd

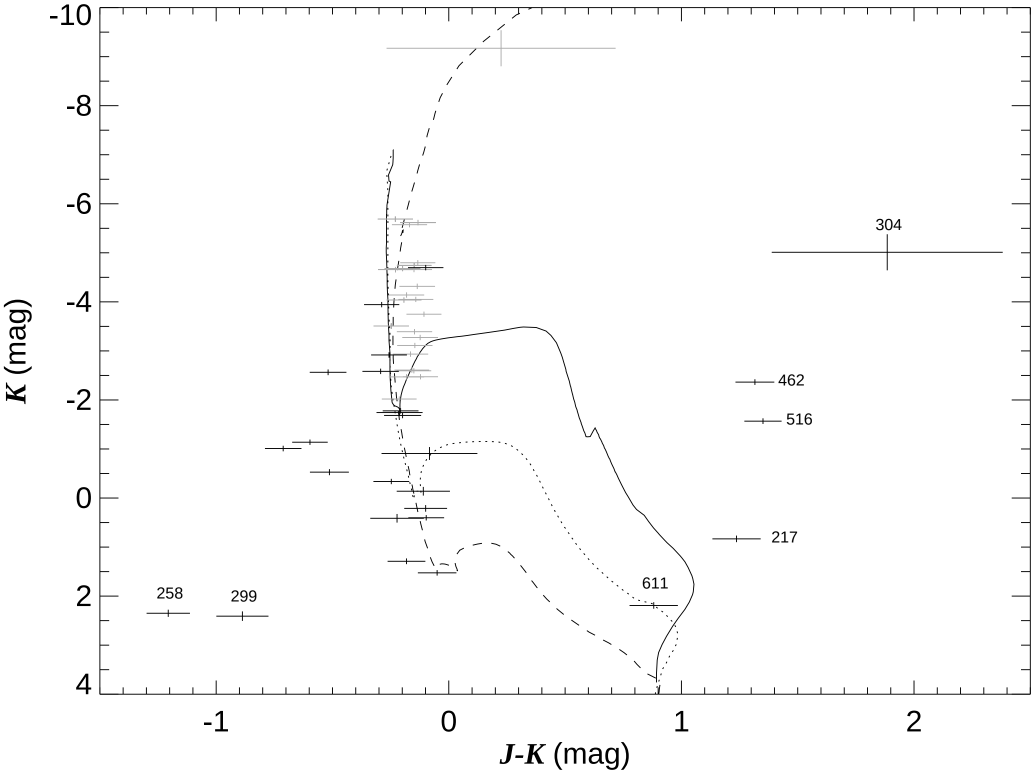

Figure 3. Color-magnitude diagram in $J - K_s$ and K_s of the probable companions (black) and their primary stars (gray), dereddened according to estimates from Negueruela et al. (2008), Massey & Thompson (1991), and Torres-Dodgen et al. (1991), and converted to absolute magnitude using a distance modulus of $DM = 10.66$. Overlaid are isochrones for ages of 0.1 Myr (solid line), 1 Myr (dotted line), and at 7 Myr (dashed line) from Bressan et al. (2012). Very blue and red companions are labeled by their primary's MT number.

of a tentatively identified star cluster (Bica et al. 2003), so it it possible that some of the companions that met the P_{ca} criterion are cluster members that are not directly orbiting the central star.

The total multiplicity fraction MF (number of targets with any companion divided by the number of targets) and companion frequency CF (total number of companions divided by the number of targets) are summarized in Table 6 with uncertainties estimated as described by Aldoretta et al. (2015). The columns list the sample, a reference code, the number of primary targets N, the range in physical separation of the detected companions given as the logarithm (base 10) of separation in Astronomical Units $\log a$, the maximum magnitude difference of companions $\triangle m$(max), MF, and CF. The top section of Table 6 lists our results and those of prior studies for companions that are angularly resolved. The lower section gives similar statistics by including closer systems discovered as spectroscopic binaries and/or eclipsing and ellipsoidal binaries (SB/E) in order to estimate the multiplicity properties over the full range of separation. The combined resolved and SB/E companion numbers are listed in column 6 of Table 5, and the resulting statistics are shown in the first row of the lower section of Table 6. The multiplicity fraction increases from $MF = 0.46$ to 0.65 by adding the known closely separated binaries, and likewise the companion frequency increases from $CF = 0.69$

Table 6. Frequency of Multiple Systems and Companion Frequency

Sample	Ref. [a]	N	$\log a$ (AU)	$\triangle m$(max) (mag)	MF	CF
Resolved Companions						
Cyg OB2	1	74	[2,4]	9	0.46 ± 0.06	0.69 ± 0.11
Cep OB2/3	2	148	[2,3]	7	0.25	0.27
Orion Trapezium	3	16	[0,3]	5	0.69	1.38
Young Stars in Upper Sco	4	91	[1,3]	10	0.27 ± 0.05	0.43 ± 0.07
Sco OB2 B-type	5	58	[0,1]	3	0.26	0.26
NGC 6611	6	60	[2,3]	6	0.18 ± 0.06	0.18 ± 0.06
Galactic OB in clusters/assoc.	7	214	[1,3]	5	0.31 ± 0.03	0.34 ± 0.04
Southern O-type	8	96	[0,4]	8	0.75 ± 0.04	1.5
Massive YSOs	9	32	[3,5]	5	0.31 ± 0.08	0.53 ± 0.09
Resolved + SB/E Companions						
Cyg OB2 (all)	10	74	[−1,4]	9	0.65 ± 0.05	1.11 ± 0.13
Cyg OB2 ($M < 25M_\odot$)	10	38	[−1,4]	9	0.66 ± 0.08	1.00 ± 0.17
Cyg OB2 ($M > 25M_\odot$)	10	27	[−1,4]	9	0.78 ± 0.08	1.56 ± 0.23
Galactic OB in clusters/assoc.	7	214	[−1,4]	5	0.69 ± 0.03	1.67 ± 0.17
Southern O-type	8	96	[−1,4]	8	0.91 ± 0.03	2.1

[a] 1. This paper and Caballero-Nieves et al. (2014); 2. Peter et al. (2012); 3. Gravity Collaboration et al. (2018); 4. Lafrenière et al. (2014); 5. Rizzuto et al. (2013); 6. Duchêne et al. (2001); 7. Aldoretta et al. (2015); 8. Sana et al. (2014); 9. Pomohaci et al. (2019); 10. This paper, Caballero-Nieves et al. (2014), and Kobulnicky et al. (2014).

to 1.11 with inclusion of the close systems. There are 29 known spectroscopic systems among our sample of stars (column 5 of Table 5), and resolved companions are more common in this subset ($MF = 15/29 = 0.52$ and $CF = 24/29 = 0.83$) than among the full sample ($MF = 0.46$ and $CF = 0.69$).

It is important to bear in mind that our reported statistics on angularly resolved binaries only include those companions above both the dotted (detection limited) and dashed lines (background limited) in Figure 1, so the MF and CF results in Table 6 should be regarded as lower limits because we miss systems outside of these limits. In particular, there is a systematic bias against detection of close and faint companions (Fig. 1). Consequently, it is very difficult to derive distributions of binary separation and mass ratio from our results. Furthermore, the magnitude-dependent characteristics of these limits may introduce some biases into our results, for example, with respect to stellar mass.

There is a well-known trend for the multiplicity fraction to increase with stellar mass (Duchêne & Kraus 2013; Sana et al. 2014), and it is worthwhile examining whether or not this trend exists within our sample of Cyg OB2 stars. We divided the stars with mass estimates (column 8 of Table 5) into those below and above $25M_\odot$, and the statistics for these groups are given for the combined resolved plus SB/E companion numbers in rows 2 and 3 of the lower section of Table 6. We see that both MF and CF are larger in the higher mass group as expected for the trend of increasing multiplicity with stellar mass. We caution, however, that this mass dependence is partially due to selections effects. We show in Figure 1 the dividing lines for meeting the $P_{ca} < 1\%$ criterion for target stars with bright and faint magnitudes. These trends show that at larger separation ρ the $P_{ca} < 1\%$ criterion will reject more and more brighter companions because of confusion with the background field. At the fainter apparent magnitude of the lower mass stars in our sample, the exclusion of candidate binaries becomes even more severe, so we expect that the multiplicity fraction will be lower for lower mass stars because of the greater difficulty in distinguishing their companions from the background stars. Consequently, the apparent increase in MF and CF with stellar mass in Table 6 is probably overestimated. Indeed, the statistics for the high mass group are probably more representative of the actual numbers, because the selection limits are more generous for the brighter, massive targets.

The upper part of Table 6 compares our multiplicity results with other earlier investigations from adaptive optics, Lucky Imaging, and interferometry. All these samples consist of massive or very young stars, similar to the composition of our Cyg OB2 sample. However, each of these surveys is sensitive to a particular range in angular separation and maximum magnitude contrast (columns 4 and 5, respectively, in Table 6), and in general those studies that cover a broader range in separation and magnitude difference yield higher multiplicity frequencies. Our results for MF and CF fall well within the range of these earlier studies, and higher values are only found from recent VLTI interferometric studies of the nearby Orion Trapezium (Gravity Collaboration et al. 2018) and southern O-type stars (Sana et al. 2014), and these studies span a relatively large range in separation and contrast sensitivity.

The lower part of Table 6 compares the statistics for the combined wide and close binary samples of Cyg OB2 with those from two all-sky surveys. Our results are broadly consistent with those from the *HST*/FGS survey of O-type stars by Aldoretta et al. (2015) for their subset of cluster and association members and with the VLTI/PIONIER and NACO/Sparse Aperture Masking survey of southern sky O-stars by Sana et al. (2014). In particular, if we adopt the results from the high mass group as the least affected by selection effects (see above), then our MF and CF results for Cyg OB2 appear to be consistent with these other surveys. Taken together, these studies imply that the massive stars in clusters and associations have a very large multiplicity frequency compared to lower mass stars (Duchêne & Kraus 2013).

The high incidence of multiple systems among the more massive stars indicates that the angular momentum of the natal cloud is preferentially transformed into orbital motion (Larson 2010). The processes involved in massive star formation are still the subject of active investigation (Rosen et al. 2020). The turbulent core model envisions the collapse of a virial natal cloud that creates widely spaced binaries accompanied by a small number of low mass stars formed by cloud fragmentation (Rosen et al. 2019). The stellar cores are surrounded by large disks, and disk fragmentation can lead to the formation of bound stellar companions (Kratter & Matzner 2006). Subsequent disk accretion onto these companions can lead to the formation of close binaries (Lund & Bonnell 2018; Tokovinin & Moe 2020) that have much smaller separations than those investigated here. Alternatively, the competitive accretion model (Bonnell & Bate 2006) suggests that massive stars form by accretion onto a cluster of low mass seeds in the dense, central regions of the natal cloud. These models tend to form star clusters where three-body encounters can create massive binaries over a wide range in separation (Wall et al. 2019). Both the turbulent core and competitive accretion models predict an increased binary fraction among more massive stars, but with somewhat different distributions in separation and mass ratio (Peter et al. 2012; Gravity Collaboration et al. 2018).

The subsequent dynamical interactions in small number clusters will generally lead to the formation a single, wide massive binary and the ejection of lower mass single stars (Griffiths et al. 2018). Wide binaries with separations of 100 to 10,000 AU are large enough for frequent gravitational encounters to occur in dense environments, and the large numbers of such wide binaries in Cyg OB2 indicates that they have survived potential disruptive encounters. Griffiths et al. (2018) argue that star formation in Cyg OB2 probably occurred in many well-separated locations in the natal cloud, so that close encounters with other cluster stars did relatively little damage to these wide binaries. This conclusion is bolstered by the fact that the binary frequency found in massive Young Stellar Objects (representing the frequency at birth) is similar to the present day binary frequency in Cyg OB2 (Table 6) even after several million years of dynamical evolution.

6. CONCLUSIONS

Our near-IR adaptive optics survey of the Cyg OB2 association has yielded astrometry and photometry for the fields surrounding 74 of its massive O- and B-type members. We find that 46% of the sample of stars have a companion that is probably physically related. These companions have projected separations in the range from 100 to 19,000 AU, and the faintest companions detected are probably $2M_\odot$ stars based upon their positions in the $(J-K, K)$ color - magnitude diagram. Many other closer companions must exist, and we included spectroscopic binary results from studies by Kobulnicky et al. (2014) that primarily sample systems with a semimajor axis range of 0.1 to 1 AU. The combined binary fraction is large even without accounting for systems in the relatively unexplored separation range of 1 to 100 AU. The derived multiplicity fraction is $MF = 0.65 \pm 0.05$ and the companion frequency is $CF = 1.11 \pm 0.13$. We emphasize that these are lower limits to the actual fractions because our observations miss both very close and faint companions and because the fainter companions are indistinguishable from background stars. Nevertheless, our results are broadly consistent with earlier surveys of massive stars that include both spectroscopic (close) and resolved (wide) binaries. For example, the HST/FGS survey of O-type stars by Aldoretta et al. (2015) yielded $MF = 0.51 - 0.69$ and $CF = 0.70 - 1.67$ among cluster and association stars, and the VLTI/PIONIER and NACO/Sparse Aperture Masking survey of O-stars by Sana et al. (2014) led to $MF = 0.91 \pm 0.03$ and $CF = 2.2 \pm 0.3$. This very high incidence of bound companions is consistent with the idea that massive star formation directs the angular momentum of the natal cloud into the creation of binary orbital motion.

The NIRI survey will help in the selection of targets for future adaptive optics and integral field unit spectroscopy observations to determine the physical properties of the companions. The close companion stars detected in the NIRI survey are especially interesting because their flux is blended into that of the main target for most ground-based observations that lack high angular resolution. Thus, the NIRI results can help correct the placement of these stars in the H-R diagram and can inform the interpretation of spectroscopy of hierarchical triples and other composite spectrum targets (see the case of MT 429; Kiminki et al. 2012). Finally, the closest resolved binaries hold the potential for orbital solutions and mass determination of the most massive stars. For example, S 5 = Cyg OB2 #5 is an hierachical system consisting of a central massive close binary, nearby tertiary, plus the two distant resolved companions (Rauw et al. 2019). The brightest and presumably most massive star in Cyg OB2 is MT 304 = Cyg OB2 #12, and both the close companion found by HST/FGS and the more distant companion found in the NIRI survey were detected in speckle observations by Maryeva et al. (2016), who claim that the close component has already displayed some orbital motion. The orbital period is probably $P \approx 100$ yr, so continued high angular resolution observations hold the promise of weighing the most massive star in Cyg OB2 and one of the most massive stars in the Galaxy.

ACKNOWLEDGMENTS

Based on observations obtained at the Gemini Observatory, (GN-2005B-Q-64, GN-2008A-Q-85, GN-2008B-Q-95) which is operated by the Association of Universities for Research in Astronomy, Inc., under a cooperative agreement with the NSF on behalf of the Gemini partnership: the National Science Foundation (United States), National Research Council (Canada), CONICYT (Chile), Ministerio de Ciencia, Tecnología e Innovación Productiva (Argentina), Ministério da Ciência, Tecnologia e Inovação (Brazil), and Korea Astronomy and Space Science Institute (Republic of Korea). We thank the staff of the Gemini North Observatory and especially Dr. Andrew Stephens for their support of this program. The data was processed using the Gemini IRAF package. This paper contains observations obtained at the Hale Telescope, Palomar Observatory. This research has made use of the Washington Double Star Catalog maintained at the U.S. Naval Observatory. This publication also made use of data products from the Two Micron All Sky Survey, which is a joint project of the University of Massachusetts and the Infrared Processing and Analysis Center/California Institute of Technology, funded by the National Aeronautics and Space Administration and the National Science Foundation. This work was directly supported by the National Science Foundation under grants AST-1009080 and AST-1411654. Institutional support has been provided from the GSU College of Arts and Sciences and from the Research Program Enhancement fund of the Board of Regents of the University System of Georgia, administered through the GSU Office of the Vice President for Research and Economic Development. A portion of the research in this paper was carried out at the Jet Propulsion Laboratory, California Institute of Technology, under a contract with the National Aeronautics and Space Administration (NASA). Financial support was provided to SCN by the Science and Technology Facilities Council for part of this work at the University of Sheffield, with current support provided by the Florida Institute of Technology. We are grateful for all this support.

Facilities:

Facility: Gemini (NIRI)

Software: FITSTARS (ten Brummelaar et al. 2000), SEextractor (Bertin & Arnouts 1996)

APPENDIX

A. NIRI/ALTAIR ASTROMETRY CALIBRATION

Each NIRI observation comes with World Coordinate System (WCS) information in the FITS header that is retained through the image reduction and coaddition process. These keywords list the pointing position and the right ascension and declination changes with pixel spacing along both axes. In principle, these can be used with the (x, y) positions of stars in the merged image that were measured with SExtractor to derive the celestial coordinates (α, δ). However, there are several complications that need to be considered. First, the pixel scale changed with the introduction of the field lens according to the Gemini Web site[4] (see Table 7), but this change was neglected in the WCS header keywords. Second, there is an apparent barrel distortion in the NIRI $f/32$ camera images that causes stars at the periphery to appear closer to the center than they should based upon a strict linear plate scale (see notes at the Gemini Web site). Finally, it is important to make an independent check on the field rotation parameter in the FITS header.

We decided to verify the pixel scales and rotational zero point through a comparison of the relative (x, y) positions with astrometry of the targets from the UK Infrared Telescope Infrared Deep Sky Survey (UKIDSS; Lawrence et al. 2007). The celestial coordinates in UKIDSS (J2000 equinox) are based upon stellar positions in the 2MASS survey (Skrutskie et al. 2006) and hence are indirectly related to the International Reference Coordinate System through the Tycho-2 system used by 2MASS (Lodieu et al. 2007).

Our goal was to obtain plate solutions for the field rotation and the x- and y-axis pixel scales from our (x, y) positions and the corresponding UKIDSS (α, δ) coordinates for as many fields as possible. The first step was to remove the barrel distortion effects. We assumed that the main target occupied the axial central position, and that the radial distance r of any other star from the image center equals the uncorrected linear distance from the main target. However, this is an approximation, because the dither pattern placed the target in the center in only one of the nine dither locations, and the star is displaced by 0 or ±50 pixels in x and y for the other dither placements. In fact, the distortion correction should actually be made before image coaddition to avoid variations in radial distance between the target and image center in the individual frames, but the dither offsets are small enough for our observations that the positional smearing that results from coaddition before barrel distortion correction only amounts to about one pixel at the edge of the FOV. The true radial distance corrected for barrel distortion is

$$r' = r + kr^2$$

where $k = (1.32 \pm 0.02) \times 10^{-5}$ and r is given in pixels (see Gemini Web site). Then the relative position from center $(\triangle x, \triangle y)$ may be transformed to a barrel distortion corrected position at

$$\triangle x' = \triangle x(r'/r) = \triangle x + k\triangle x(\triangle x^2 + \triangle y^2)^{1/2}$$

and

$$\triangle y' = \triangle y + k\triangle y(\triangle x^2 + \triangle y^2)^{1/2}.$$

Next we obtained UKIDSS K-band source data for the nominal position of the main target (from 2MASS) using a 15 arcsec search radius[5]. The stellar positions were extracted from the UKIDSSDR7PLUS data release of the UKIDSS Galactic Plane Survey. We used the preliminary WCS header data to transform (x, y) to (α, δ) to then match our targets with the sources in UKIDSS (where possible) based upon similar coordinates and magnitudes. Finally, we used the positional and coordinate data to obtain a plate solution using the IDL procedure astromit.pro (written by R. Cornett and W. Landsman[6]). The results for each field were collected in a file that listed the rotation angle and pixel scale in x and y for both the preliminary WCS data and the fit of the UKIDSS coordinates, plus the number of stars used in the fit.

---

[4] http://www.gemini.edu/sciops/instruments/niri/imaging/pixel-scales-and-fov

[5] http://surveys.roe.ac.uk:8080/wsa/region_form.jsp

[6] http://www.astro.washington.edu/docs/idl/idllib/obsolete/sunuit/lib/old/astromit.pro

Table 7. Astrometric Scales for the NIRI/ALTAIR $f/32$ Camera

Parameter	Field lens out	Field lens in
Pixel scale [Gemini WWW] (mas pix^{-1})	21.9	21.4
Pixel scale [Stoesz 2006] (mas pix^{-1})	21.8 ± 0.2	21.4 ± 0.2
Pixel scale [WCS] (mas pix^{-1})	21.859 ± 0.012	21.860 ± 0.003
Pixel scale [fit] (mas pix^{-1})	21.781 ± 0.025	21.298 ± 0.008
WCS scale factor from fit	0.9964 ± 0.0013	0.9743 ± 0.0004
$\triangle\theta$ (deg)	0.59 ± 0.12	0.40 ± 0.03
Number of fields	6	43

We found that there were 49 fields where four or more stars were matched by sources in UKIDSS, and we used these to determine mean values of the pixel scales and rotational offsets that are summarized in Table 7 according to the field lens position (out for the 2005 observations and in for those from 2008). The first two rows give the expected pixel scales from the Gemini Web site and the work of Stoesz (2006), and the next two rows show the average of the x and y pixel scales according to the preliminary WCS keywords and the fit of the UKIDSS astrometry, respectively. The uncertainties quoted are the standard deviations of the mean in each case. We see that the pixel scales are close to the expected values, and the ratio of the fitted to WCS pixel scales (given in the fifth row as the WCS scale factor) is slightly less than one. Finally, there is a small but non-zero offset between the field rotational angle θ from the preliminary WCS keyword and the fits of the UKIDSS astrometry, $\triangle\theta = \theta(\text{UKIDSS}) - \theta(\text{WCS})$.

We used these calibration results to determine the (x, y) to (α, δ) transformation using the IDL procedure xyad.pro[7] (written by W. Landsman) that we modified by performing the barrel distortion correction (see above), making a small rotation of the $(\triangle x', \triangle y')$ positions using $\triangle\theta$ for the lens in/out solutions in Table 7, and then rescaling the WCS pixel scales using the WCS scale factors for the lens in/out solutions in Table 7. The relative coordinates were then transformed to absolute (α, δ) using the 2MASS coordinates for the main target (J2000 equinox and ignoring the effects of proper motion between the times of the 2MASS survey and our observations). We caution that in some cases the 2MASS coordinates may actually represent the center of light position between the main target and a close companion, so that in such cases all the (α, δ) estimates may have systematic offsets. The relative positions (ρ, θ) should be regarded as our fundamental astrometric measurements. The target MT421 (Cyg OB2-22) was also observed by Maíz Apellániz (2010) using the Advanced Camera for Surveys (ACS) High Resolution Camera (HRC) on *Hubble Space Telescope* (red F850LP filter), and we compared the separations and position angles of the companions observed with *HST* and our calibrated astrometry to verify our calibration process. We found that the mean difference in fractional separation for five companions was 0.0011 ± 0.0023 and the mean difference in position angle was 0.11 ± 0.15 deg. Thus, our calibration of the astrometry leads to pixel scales that agree at the 0.1% level and to systematic rotational differences at the 0.1 deg level. The standard deviation between the rectilinear positions from the *HST* and NIRI astrometry is about 0.008 arcsec for these five companion stars, and this may represent the magnitude of any high-order geometric distortions that may exist in the NIRI ALTAIR astrometry system.

B. NIRI/ALTAIR PHOTOMETRY CALIBRATION

The NIRI/ALTAIR images suffer from angular anisoplanatism that causes the point-spread function (PSF) to change from the center to the edge of the image. Stellar images near the periphery have relatively more flux in the halo surrounding the core than does a star image at the center. We measured stellar fluxes using aperture photometry with SExtractor for a series of apertures with diameters ranging from 5 to 80 pixels, and these represent a radial integration of the stellar PSF. Figure 4 shows an encircled energy (EE) plot of total flux measured versus aperture diameter for the case of a 2005 K-band observation of MT 465. The solid line represents the EE curve for the target at the center of image and the dotted line shows the EE curve for another star offset by 431 pixels from the main target. We see that the PSF degradation of the offset star image results in a relative reduction in measured flux that is larger at smaller aperture size. Consequently, if we adopted a fixed aperture diameter of say 10 pixels for all our measurements, then we would systematically underestimate the flux of stars towards the edge of the field. On the other hand, if we used a larger diameter aperture (60 pixels or larger), then the differences in the EE flux with position would be insignificant. Unfortunately, the large aperture option is only practical with the brightest and isolated stars because the stellar signal becomes overwhelmed by background noise for faint stars measured with large apertures (often causing the EE curve to decline with increasing aperture; Howell 1989). Hence, we must apply an aperture correction scheme that accounts for the PSF degradation of our measurements.

The amount of PSF degradation depends on the radial position of the star, the jitter introduced by the coaddition of the individual frames, whether or not the NIRI field lens was used, and the air

---

[7] http://idlastro.gsfc.nasa.gov/ftp/pro/astrom/xyad.pro

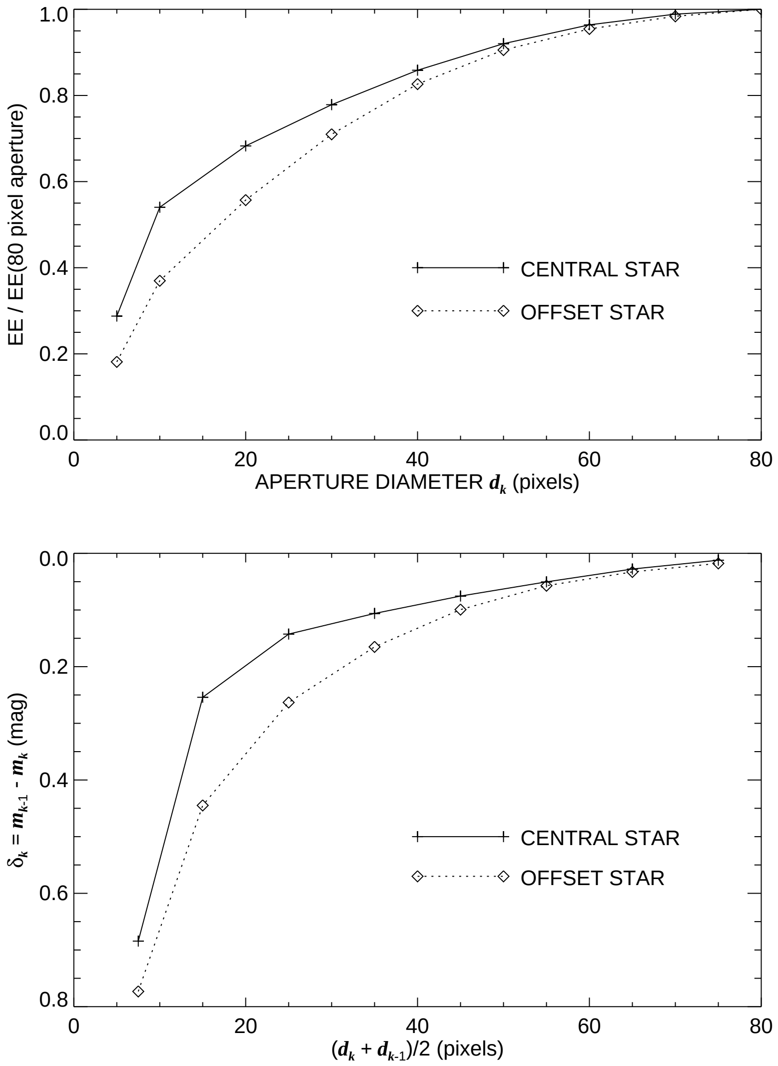

Figure 4. Above: A plot of encircled energy (EE) versus aperture diameter for MT 465 (solid line) and a companion star near the edge (dotted line). Both are normalized by the encircled energy for an aperture with a 80 pixel diameter. Below: The difference in measured instrumental magnitude between sequential apertures of diameters d_{k-1} and d_k plotted versus the mean of these diameters.

mass and seeing conditions at the time of the observation. Cresci et al. (2005) argue that a first order correction can be made for PSF degradation by considering a family of PSFs characterized by the ratio of the offset angle to the isoplanatic angle (dependent on air mass and seeing). Because the isoplanatic angle is inversely proportional to the astronomical seeing, this suggests that we may parameterize the changes in the EE curves using a parameter $\alpha \equiv r\theta_s$, where r is the offset position from the target at the center of the image (measured in pixels) and θ_s is the FWHM of the astronomical seeing (recorded in the NIRI/ALTAIR header files as keyword `AOSEEING`). We first tested this idea by calculating EE curves for synthetic PSFs for NIRI/ALTAIR created with the PAOLA software package (Jolissaint 2010), and we found that the ratio $EE_k/EE_k[\mathrm{REF}]$ (where EE_k is the normalized enclosed energy for aperture k and EE_k[REF] is the same for the main target at center) did indeed decline in an approximately linear fashion with both increases in radial offset and seeing. However, the observed PSFs have sufficiently different core structure from the model PSFs (presumably due to jitter that is not included in the models) that we decided to calibrate the change in the EE curves directly from our observations.

We implemented the aperture correction using the differential magnitude approach outlined by Stetson (1990) in which the instrumental magnitude difference between two apertures is

$$\delta_k = -2.5 \log(F_k/F_{k-1})$$

where F_k is the flux estimated by SExtractor for an aperture of diameter d_k. Uncertainties in δ_k were set by the flux uncertainties according to the S/N from equation (1) of Howell (1989). This differential version of the EE curve is shown in the lower part of Figure 4. The advantange of using the differential form δ_k is that this magnitude difference may be estimated for the smaller apertures even for those faint stars where the EE curve is unreliable at larger apertures because of background noise (Stetson 1990).

We then gathered δ_k measurements for all the aperture pairs for image samples selected by date (to account for the use or not of the field lens) and by filter band. In each case we formed the difference between δ_k for a given star and that for the central reference target, and we collected the offset parameter $\alpha = r\theta_s$. The uncertainties in $\alpha = r\theta_s$ are estimated as ±15%, which reflects the typical scatter in seeing estimates among the subexposures. An uncertainty weighted fit was made of the function

$$\delta_k - \delta_k(\mathrm{REF}) = a_k\alpha$$

for the first-order model of PSF degradation with parameter α. The derived constants a_k and their uncertainties are collected in Table 8 for each year and filter sample. The second row in the header indicates the associated aperture pair (by diameter in pixels) for each column. The PSF degradation trends are largest in the smaller aperture pairs, shorter wavelength filters, and data from 2005 when the AO field lens was not used. We also list in Table 8 similar coefficients for the PSF degradation observed in the PHARO images (made in 2009), but these should not be directly compared with the NIRI/ALTAIR results because the pixel scale is different and no seeing estimate was reported at the time, but based on AO performance, we estimate the data were taken in approximately $0.8''$ seeing (Dekany et al. 2007).

Table 8. PSF Degradation Correction Coefficients and Approximation Uncertainties

Image Set	$a_1 \times 10^6$ (5–10)	$a_2 \times 10^6$ (10–20)	$a_3 \times 10^6$ (20–30)	$a_4 \times 10^6$ (30–40)	$a_5 \times 10^6$ (40–50)	$a_6 \times 10^6$ (50–60)	$a_7 \times 10^6$ (60–70)	$a_8 \times 10^6$ (70–80)
2005 J	1130 ± 46	1095 ± 28	169 ± 20	65 ± 18	30 ± 17	-11 ± 16	-25 ± 16	-32 ± 16
2005 H	677 ± 47	960 ± 33	473 ± 27	104 ± 25	34 ± 24	15 ± 24	-2 ± 26	0 ± 28
2005 K	287 ± 50	770 ± 35	465 ± 29	223 ± 27	104 ± 32	40 ± 35	-5 ± 41	7 ± 27
2008 J	976 ± 23	896 ± 15	251 ± 12	72 ± 10	22 ± 9	-53 ± 9	-67 ± 10	-42 ± 10
2008 K	4 ± 19	510 ± 14	225 ± 14	69 ± 14	39 ± 14	17 ± 16	-20 ± 16	-33 ± 15
2009 J	166 ± 25	326 ± 18	110 ± 16	44 ± 16	81 ± 14	23 ± 12	17 ± 16	32 ± 17
2009 H	289 ± 17	297 ± 11	112 ± 10	28 ± 10	10 ± 9	-23 ± 9	-5 ± 9	16 ± 9
2009 K_S	176 ± 15	56 ± 10	84 ± 9	25 ± 9	4 ± 9	0 ± 9	-1 ± 9	-20 ± 9
$\sigma(\delta_k[\mathrm{MODEL}])$ (mag)	0.162	0.049	0.022	0.010	0.009	0.010	0.014	0.017

NOTE—Any negative values are assigned zero in practice.

We used the observed PSF degradation trends to estimate a model differential magnitude curve δ_k for each target's position according to

$$\delta_k = \delta_k[\mathrm{REF}] + a_k\alpha$$

where δ_k[REF] is the magnitude difference between apertures $k-1$ and k for the central reference star, a_k is the coefficient for a given date and filter (given in Table 8), and $\alpha = r\theta_s$ is the radial distance – seeing product. It is important to check how well this approximate treatment works in practice, so we compared the predicted curve δ_k[MODEL] with those observed for a subsample of 16 very bright and radially offset stars where the uncertainties due to photon and background noise are insignificant. The standard deviations of the observed minus model δ_k curves, $\sigma(\delta_k[\mathrm{MODEL}])$, are given with each entry in Table 8, and these represent how well we might expect the model to perform in our application. In general these standard deviations are small but they are worse for the smallest aperture pairs where structure variations in the PSF are most pronounced. The full uncertainty in our δ_k estimate is given by

$$\sigma^2(\delta_k) = \sigma^2(\delta_k[\mathrm{MODEL}]) + \sigma^2(\delta_k[\mathrm{REF}]) + \sigma^2(a_k\alpha)$$

where the final term accounting for the off-axis correction is

$$\sigma^2(a_k\alpha) = (a_k\alpha)^2\left(\left(\frac{\sigma(a_k)}{a_k}\right)^2 + \left(\frac{\sigma(\alpha)}{\alpha}\right)^2\right) \approx \alpha^2\left(\sigma(a_k)^2 + a_k^2\left(\frac{\sigma(\theta_s)}{\theta_s}\right)^2\right).$$

The approximation used in the last step assumes that all the uncertainty in the $\alpha = r\theta_s$ product stems from the seeing uncertainty $\sigma(\theta_s)$. The uncertainties in the coefficients $\sigma(a_k)$ are given with each entry of Table 8, and we adopt $\sigma(\theta_s)/\theta_s = 0.15$.

Now with the off-axis aperture curves δ_k in hand, we may estimate the magnitude difference between target and central reference star using an aperture correction as given by

$$\triangle m_k = -2.5\log(F_k/F_{80}[\mathrm{REF}]) - \sum_k^8 \delta_k$$

where we refer all the fluxes to that in the largest, 80 pixel diameter aperture of the reference star. The uncertainty associated with this magnitude difference is

$$\sigma^2(\triangle m_k) = \sigma^2(F_k) + \sum_k^8 \sigma^2(\delta_k)$$

where $\sigma(F_k)$ is the uncertainty in the flux measurement expressed as a magnitude and $\sigma(\delta_k)$ are the uncertainties in the adopted δ_k curve as given above. Thus, we arrive at nine estimates of the magnitude difference and associated uncertainty from the measurements made in nine apertures. We select the estimate with the smallest uncertainty for our purposes in this paper, so that we can adopt the best compromise between large apertures for the bright stars (where the flux uncertainties are small compared to the aperture correction uncertainties) and smaller apertures for the fainter stars (where the flux uncertainties become huge in the large apertures). Note that stars at the periphery of the fields (i.e. stars that were not in all frames due to dithering) will have larger uncertainties than reported in Table 4.

We checked our scheme by comparing our derived differential K-band magnitudes with those from the UKIDSS catalog for the populous field surrounding star MT 421. The individual stars were matched between the NIRI and UKIDSS sources according to our astrometry solution. Unfortunately, MT 421 itself is saturated in the UKIDSS data, so it is not possible to form magnitude differences from the UKIDSS data alone. Instead, we found the best fit magnitude offset needed to match the NIRI magnitude differences, and the implied K magnitude of MT 421 is $K = 7.77$ which is similar to the estimate from 2MASS, $K = 7.76$. We find that our corrected magnitudes and those from UKIDSS are in satisfying agreement with no evidence of systematic differences with magnitude. Furthermore, the scatter about the expected one-to-one relation is comparable to our uncertainty estimates, which suggests that our analytical representation of the uncertainties is reliable.

REFERENCES

Albacete Colombo, J. F., Caramazza, M., Flaccomio, E., Micela, G., & Sciortino, S. 2007, A&A, 474, 495

Aldoretta, E. J., Caballero-Nieves, S. M., Gies, D. R., et al. 2015, AJ, 149, 26

Bertin, E., & Arnouts, S. 1996, A&AS, 117, 393

Bica, E., Bonatto, C., & Dutra, C. M. 2003, A&A, 405, 991

Bonnell, I. A., & Bate, M. R. 2006, MNRAS, 370, 488

Bressan, A., Marigo, P., Girardi, L., et al. 2012, MNRAS, 427, 127

Caballero-Nieves, S. M., Nelan, E. P., Gies, D. R., et al. 2014, AJ, 147, 40

Comerón, F., Pasquali, A., Figueras, F., & Torra, J. 2008, A&A, 486, 453

Comerón, F., Pasquali, A., Rodighiero, G., et al. 2002, A&A, 389, 874

Correia, S., Zinnecker, H., Ratzka, T., & Sterzik, M. F. 2006, A&A, 459, 909

Cresci, G., Davies, R. I., Baker, A. J., & Lehnert, M. D. 2005, A&A, 438, 757

Czekaj, M. A., Robin, A. C., Figueras, F., Luri, X., & Haywood, M. 2014, A&A, 564, A102

Dekany, R., Bouchez, A., Roberts, J., et al. 2007, in Advanced Maui Optical and Space Surveillance Technologies Conference, E64

Dekany, R., Roberts, J., Burruss, R., et al. 2013, ApJ, 776, 130

Duchêne, G., & Kraus, A. 2013, ARA&A, 51, 269

Duchêne, G., Simon, T., Eislöffel, J., & Bouvier, J. 2001, A&A, 379, 147

Fitzpatrick, E. L. 1999, PASP, 111, 63

Gravity Collaboration, Karl, M., Pfuhl, O., et al. 2018, A&A, 620, A116

Griffiths, D. W., Goodwin, S. P., & Caballero-Nieves, S. M. 2018, MNRAS, 476, 2493

Hanson, M. M. 2003, ApJ, 597, 957

Hayward, T. L., Brandl, B., Pirger, B., et al. 2001, PASP, 113, 105

Hodapp, K. W., Jensen, J. B., Irwin, E. M., et al. 2003, PASP, 115, 1388

Howell, S. B. 1989, PASP, 101, 616

Jolissaint, L. 2010, Journal of the European Optical Society, 5

Kiminki, D. C., Kobulnicky, H. A., Vargas Álvarez, C. A., Alexander, M. J., & Lundquist, M. J. 2015, ApJ, 811, 85

Kiminki, D. C., Kobulnicky, H. A., Kinemuchi, K., et al. 2007, ApJ, 664, 1102

Kiminki, D. C., Kobulnicky, H. A., Ewing, I., et al. 2012, ApJ, 747, 41

Kobulnicky, H. A., Smullen, R. A., Kiminki, D. C., et al. 2012, ArXiv e-prints

Kobulnicky, H. A., Kiminki, D. C., Lundquist, M. J., et al. 2014, ApJS, 213, 34

Kratter, K. M., & Matzner, C. D. 2006, MNRAS, 373, 1563

Lafrenière, D., Jayawardhana, R., van Kerkwijk, M. H., Brandeker, A., & Janson, M. 2014, ApJ, 785, 47

Larson, R. B. 2010, Reports on Progress in Physics, 73, 014901

Lawrence, A., Warren, S. J., Almaini, O., et al. 2007, MNRAS, 379, 1599

Le Bouquin, J. B., Sana, H., Gosset, E., et al. 2017, A&A, 601, A34

Lodieu, N., Hambly, N. C., Jameson, R. F., et al. 2007, MNRAS, 374, 372

Lund, K., & Bonnell, I. A. 2018, MNRAS, 479, 2235

Maíz Apellániz, J. 2010, A&A, 518, A1

Maíz Apellániz, J., Sota, A., Arias, J. I., et al. 2016, ApJS, 224, 4

Maíz Apellániz, J., Trigueros Páez, E., Negueruela, I., et al. 2019, A&A, 626, A20

Maryeva, O. V., Chentsov, E. L., Goranskij, V. P., et al. 2016, MNRAS, 458, 491

Mason, B. D., Hartkopf, W. I., Gies, D. R., Henry, T. J., & Helsel, J. W. 2009, AJ, 137, 3358

Mason, B. D., Wycoff, G. L., Hartkopf, W. I., Douglass, G. G., & Worley, C. E. 2001, AJ, 122, 3466

Massey, P., & Thompson, A. B. 1991, AJ, 101, 1408

Muntean, V., Moffat, A. F. J., Chené, A. N., & de La Chevrotière, A. 2009, MNRAS, 399, 1977

Negueruela, I., Marco, A., Herrero, A., & Clark, J. S. 2008, A&A, 487, 575

Peter, D., Feldt, M., Henning, T., & Hormuth, F. 2012, A&A, 538, A74

Pomohaci, R., Oudmaijer, R. D., & Goodwin, S. P. 2019, MNRAS, 484, 226

Raghavan, D., McAlister, H. A., Henry, T. J., et al. 2010, ApJS, 190, 1

Rauw, G., Nazé, Y., & Campos, F. 2019, A&A, 627, A2

Richardson, E. H., Fletcher, J. M., Morbey, C. L., Oschmann, J. M., & Pazder, J. S. 1998, in Proc. SPIE, Vol. 3353, Adaptive Optical System Technologies, ed. D. Bonaccini & R. K. Tyson, 600–610

Rizzuto, A. C., Ireland, M. J., Robertson, J. G., et al. 2013, MNRAS, 436, 1694

Roberts, S., & Singh, G. 1998a, in Adaptive Optical System Technologies, Vol. 3353, 611–620

Roberts, S., & Singh, G. 1998b, in Society of Photo-Optical Instrumentation Engineers (SPIE) Conference Series, Vol. 3353, Proc. SPIE, ed. D. Bonaccini & R. K. Tyson, 611–620

Rosen, A. L., Li, P. S., Zhang, Q., & Burkhart, B. 2019, ApJ, 887, 108

Rosen, A. L., Offner, S. S. R., Sadavoy, S. I., et al. 2020, SSRv, 216, 62

Rygl, K. L. J., Brunthaler, A., Sanna, A., et al. 2012, A&A, 539, A79

Sana, H., de Mink, S. E., de Koter, A., et al. 2012, Science, 337, 444

Sana, H., de Koter, A., de Mink, S. E., et al. 2013, A&A, 550, A107

Sana, H., Le Bouquin, J.-B., Lacour, S., et al. 2014, ApJS, 215, 15

Schulte, D. H. 1958, ApJ, 128, 41

Skrutskie, M. F., Cutri, R. M., Stiening, R., et al. 2006, AJ, 131, 1163

Stetson, P. B. 1990, PASP, 102, 932

Stoesz, J. A. 2006, PhD thesis, University of Victoria, Canada

Straižys, V., & Laugalys, V. 2008, Baltic Astronomy, 17, 143

ten Brummelaar, T., Mason, B. D., McAlister, H. A., et al. 2000, AJ, 119, 2403

ten Brummelaar, T. A., Mason, B. D., Bagnuolo, Jr., W. G., et al. 1996, AJ, 112, 1180

Tokovinin, A., & Moe, M. 2020, MNRAS, 491, 5158

Torres-Dodgen, A. V., Carroll, M., & Tapia, M. 1991, MNRAS, 249, 1

van der Hucht, K. A. 2001, NewAR, 45, 135

Wall, J. E., McMillan, S. L. W., Mac Low, M.-M., Klessen, R. S., & Portegies Zwart, S. 2019, ApJ, 887, 62

Wright, N. J., & Drake, J. J. 2009, ApJS, 184, 84

Wright, N. J., Drake, J. J., Drew, J. E., et al. 2012, ApJL, 746, L21

Wright, N. J., Drew, J. E., & Mohr-Smith, M. 2015, MNRAS, 449, 741

Zinnecker, H., & Yorke, H. W. 2007, ARA&A, 45, 481